INTERNATIONAL JOURNAL FOR NUMERICAL METHODS IN FLUIDS
Int. J. Numer. Meth. Fluids 2001; **36**: 205–247

Numerical simulation of tidal bore in Hangzhou Gulf and Qiantangjiang

M. D. Su[a,*], X. Xu[a], J. L. Zhu[a] and Y. C. Hon[b]

[a] *Department of Engineering and Mechanics, Tsinghua University, Beijing, China*
[b] *Department of Mathematics, City University of Hong Kong, Hong Kong, China*

SUMMARY

In this paper, a new numerical model, based on a set of non-linear shallow water equations is developed for the simulation of the formation and evolution of tidal bore in the Hangzhou Gulf and Qiantangjiang river of China. The numerical method and boundary conditions are described in detail. The method is validated against analytical solutions and experimental data. Simulation of the actual tidal bore in Hangzhou Gulf and its propagation in the Qiantangjiang river are performed. Numerical results show that this proposed method is effective for the prediction of tidal bore and current flow at the entrance of Qiantangjiang river. Copyright © 2001 John Wiley & Sons, Ltd.

KEY WORDS: numerical simulation; shallow water equations; tidal bore

1. INTRODUCTION

The Qiantangjiang river lies along the Hangzhou Gulf, which faces the East Sea of China. It is well known for its formation of high tidal bore which marches into the Qiantangjiang river. The scene has become a famous sight-seeing point and attracts thousands of tourists annually. It is, however, potentially hazardous to the residents living along the Qiantangjiang river. Therefore, attempts to govern the channel of the Qiantangjiang river have never stopped for thousands of years. Similar tidal bores can be found elsewhere in the world. The other famous tidal bores are the Amazon bore called *pororoca*, the tidal bore on the Seine river (*mascaret*), the Hoogly bore on the Gange river and the bore on the Mekong river, etc. Smaller but also well-known tidal bores are the Severn bore near Bristol, the tidal bores on the Garonne and Dordogne rivers and the bores at the Bay of Fundy, Canada (http://www.uq.edu.au/∼e2hchans/e2320.html/#Surge and bores).

To efficiently control the danger of the tidal bore, it is necessary to understand the full process of its formation, development, propagation and dissipation. However, previous results

* Correspondence to: Department of Architecture, Massachusetts Institute of Technology, Room 5-418, 77 Massachusetts Avenue, Cambridge, MA 02319-4307, U.S.A.

Received May 1999
Revised March 2000

from field observation and numerical simulation are not complete. There are still many issues that need to be resoled for understanding and predicting the tidal bore. As we know, the riverbed of Qiangtanjiang and Hangzhou Gulf is variable and very complex. Moreover, accurate field data are very difficult to obtain because it is dangerous due to the high height and twinkling variation of the tidal bore. Therefore, methods of both observation and numerical simulation should be further developed and improved.

Recent advances in numerical modelling and computer hardware have made robust and efficient numerical models available. These models provide sufficient spatial details to simulate tidal hydrodynamic processes in gulfs and estuaries. A verified numerical hydrodynamic model is a powerful tool for providing insight into transport processes. To analyse the tidal bore by numerical methods, the finite element method and/or the finite difference method are extensively used. The major finite difference methods in solving shallow water equations can be divided into two categories: the characteristic method developed by Matsoukis [1] and Tan and Han [2], and the explicit/implicit finite difference method of Casulli [3], Fennema and Chaudhry [4,5] and Spitaleri and Corinaldesi [6]. These methods are based on rectangular grids and can only be approximately used in the numerical simulation of tidal bore in bays and estuaries that have complex geometries. Modelling of steep waves is generally very difficult. Fennema and Chaudhry [5] used two explicit second-order finite difference schemes to solve the transient shallow water equations. Although damping is less severe than for the Beam and Warming schemes, the explicit scheme is less robust than the Beam and Warming scheme of tail water to reservoir depth ratio, failing at a ratio of 0.2–0.5. The other is the finite element method (e.g. Walters [7], Westerink *et al.* [8–12], Toshio *et al.* [13], Kolar *et al.* [14]). Actually, many of the same themes that finite difference modellers are examining are also being pursued by finite element modellers. The finite element is convenient for complex geometries; however, in this method the established algebraic equations are non-linear and have to be solved by the gradient method and iteration process. Moreover, the boundary conditions and grid structure have a great influence on the numerical results. Therefore, they are also extensively discussed by Westerink *et al.* [10–12], Kolar *et al.* [15] and Lardner [16], as well as by Peterson *et al.* [17]. Although many models have been developed, the surface flow modelling is not a solved problem and much work remains. One of the difficult problems is to solve the shallow water equation with discontinuity by using both above numerical methods. However, the tidal bore in the Qiantangjiang river has a strong discontinuity. Thus, we have to develop another new method to capture it.

As we know, the performance of the shallow water equation is similar to that of the compressible Euler equation in aerodynamics. Recently, many numerical methods to capture the discontinuity, i.e. shock wave in airflow, have been developed. These methods can be applied in solving the shallow water wave, including the case with stronger discontinuity. In this paper, a new non-oscillatory and non-free dissipation (NND) parameter difference scheme [18] is proposed to simulate the full process, including its formation and evolution of the tidal bore. This proposed scheme is efficient in 'catching' the surge (sudden change of water depth, i.e. discontinuous water level) of the tidal bore. In particular, the scheme performs well with the use of unstructured meshes for fitting the irregular boundaries. In the Hangzhou Gulf, e.g. near Kanpu (see Figure 1), the water region is very wide and the waves move in different directions and speeds in the gulf. The computational region has to be two-dimensional for a

Figure 1. Map of Qiantangjiang river.

better description of the tidal bore. In the Qiantangjiang river, e.g. before Yanguan, the water region is almost a uniform channel and the wave movement can be treated as a one-dimensional flow. The subject of the present paper is to develop a mathematical model by using the NND scheme and an unstructured grid combining different methods that handle with the boundary conditions.

The present paper consists of the following: in Section 2 the one- and two-dimensional shallow water wave equations in conservation form are written. In Section 3 the basic idea of the NND scheme and its detailed deduction are given. In the one-dimensional simulation, an adaptive grid is used to improve numerical accuracy. Also, the real geometrical depth of the riverbed is used in the simulation to indicate the influence of the depth to the tidal bore. In the two-dimensional case, a new discrete method is developed to take care of the use of the unstructured mesh. To establish the discrete numerical formula, the finite volume method based on the conservation principle of momentum and mass is used. The boundary conditions at the upstream and the downstream are formulated by using characteristic analysis and non-reflective requirements. Finally, Sections 4 and 5 present numerical simulations for cases in one- and two-dimensional space respectively. Comparisons between the numerical solution, the analytical solution and real experimental data are given in Section 6, with conclusions presented in Section 7.

2. PRINCIPAL EQUATIONS

2.1. One-dimensional

In the engineering numerical simulation of long wave movement in a river, the one-dimensional Saint-Venant equation is used as the principal equation, in which the chromatic dispersion is not considered. It is a non-linear shallow wave equation, which can be written in the form (see Reference [19])

$$A_t + Q_x = 0 \tag{1}$$

$$Q_t + 2uQ_x + gA\zeta_x = u^2A_x - gAS_f \tag{2}$$

In the above, A is the area of the river cross-section under the water free surface whose breadth is B, C is the Chezy coefficient, g is the acceleration of gravity, Q is flux, u is average flow speed ($= Q/A$), ζ is the level of water free surface, x is the natural co-ordinate along the river and t is time. The definition of other geometrical parameters can be found in Figure 2. In Equation (2)

$$S_f = \frac{B}{A}\frac{u|u|}{C^2}$$

To ensure the conservation of computation, the principal equation is rewritten in the conservation form

$$\frac{\partial U}{\partial t} + \frac{\partial F}{\partial x} = H_0 \tag{3}$$

where

$$U = \{A, Q\}^T, \quad F = \left\{Q, \frac{Q^2}{A} + gI\right\}^T, \quad H_0 = \{0, R + gA(S_0 - S_f)\}^T,$$
$$I = \int_0^h (h-\eta)b(x,\eta)\,\mathrm{d}\eta, \quad R = g\int_0^h (h-\eta)\frac{\partial b(x,\eta)}{\partial x}\,\mathrm{d}\eta, \quad S_0 = -\frac{\mathrm{d}z_b}{\mathrm{d}x} \tag{4}$$

There are some tributaries that have some influences on the evolution of the water level of the Qiantangjiang river. Therefore, the equations are rewritten in the following form in order to consider their influence:

$$A_t + Q_x = \sigma \tag{5}$$

$$Q_t + 2uQ_x + gA\zeta_x = u^2A_x - gAS_f + \sigma u' \tag{6}$$

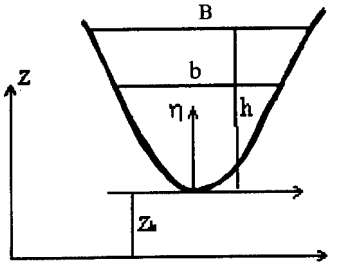

Figure 2. Sketch of river section.

where σ is the tributary flux per length along the river, $\sigma = \mathrm{d}Q'/\mathrm{d}x$; Q' is the tributary flux; u' is the tributary flow velocity component in the x-direction at the entrance (see Figure 3).

2.2. Two-dimensional

The control equations of the tidal bore are two-dimensional shallow water wave equations, i.e. Saint-Venant equations. Here, an equation of kinematic energy derived by momentum equations is added to the control equations and the control equations are rewritten in conservative form

$$\frac{\partial U}{\partial t} + \frac{\partial F}{\partial x} + \frac{\partial G}{\partial y} = H \tag{7}$$

where

$$U = \begin{bmatrix} h \\ hu \\ hv \\ e \end{bmatrix}, \quad F = \begin{bmatrix} hu \\ hu^2 + gh^2/2 \\ uvh \\ u(e+p) \end{bmatrix}, \quad G = \begin{bmatrix} hv \\ uvh \\ hv^2 + gh^2/2 \\ v(e+p) \end{bmatrix}, \quad H = \begin{bmatrix} 0 \\ gh(S_x - S_{fx}) \\ gh(S_y - S_{fy}) \\ \bar{Q} \end{bmatrix}$$

where h is water depth; u, v are velocity components in the x-, y-directions; S_x, S_y are slopes of the riverbed in the x-, y-directions (c is the propagation speed of shallow water wave)

$$e = \frac{1}{2}(u^2 + v^2 + c^2)h; \quad p = \frac{c^2 h}{2}; \quad c = \sqrt{gh}; \quad \bar{Q} = uQ_x + vQ_y$$

S_{fx}, S_{fy} are fictions on the riverbed and calculated by Manning formulations

$$S_{fx} = \frac{u\sqrt{u^2 + v^2}}{hC^2}, \qquad S_{fy} = \frac{v\sqrt{u^2 + v^2}}{hC^2} \tag{8}$$

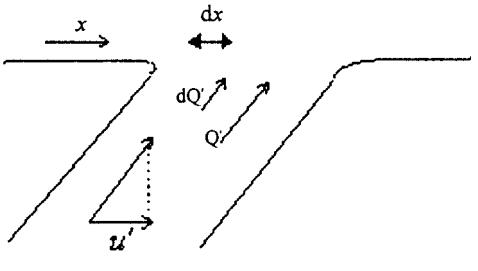

Figure 3. Parameters of tributary.

It is easy to verify

$$AU = \frac{\partial F}{\partial U} U = \begin{pmatrix} 0 & 1 & 0 & 0 \\ -u^2 + \dfrac{u^2+v^2}{2} & u & -v & 1 \\ -uv & v & u & 0 \\ -\dfrac{2eu}{h} + (u^2+v^2)u & \dfrac{2eu}{h} - \dfrac{3u^2+v^2}{2} & -uv & 2u \end{pmatrix} \begin{pmatrix} h \\ hu \\ hv \\ e \end{pmatrix} = \begin{pmatrix} hu \\ hu + \dfrac{h^2 g}{2} \\ uvh \\ u(e+P) \end{pmatrix}$$

$$= F$$

$$BU = \frac{\partial G}{\partial U} U = \begin{pmatrix} 1 & 1 & 0 & 0 \\ -uv & v & u & 1 \\ -u^2 + \dfrac{u^2+v^2}{2} & -u & v & 0 \\ -\dfrac{2ev}{h} + (u^2+v^2)v & -uv & \dfrac{2ev}{h} - \dfrac{3u^2+v^2}{2} & 2v \end{pmatrix} \begin{pmatrix} h \\ hu \\ hv \\ e \end{pmatrix} = \begin{pmatrix} hu \\ uvh \\ hu + \dfrac{h^2 g}{2} \\ v(e+P) \end{pmatrix}$$

$$= G$$

The eigenvalues of A and B are

$$\lambda(A) = \{u + c, u, u, u - c\}, \qquad \lambda(B) = \{v + c, v, v, v - c\} \tag{9}$$

It is clear that the duplicate eigenvalues u and v are produced due to the addition of the equation of kinematic energy. The duplicate eigenvalues do not change the performance of the characteristic of A and B. In fact, the fourth equation (kinematic energy equation) is not independent and it does not need to be solved. The purpose of adding this equation is to satisfy the following relations:

$$\frac{\partial F}{\partial U} U = AU = F, \qquad \frac{\partial G}{\partial U} U = BU = G; \quad A = \frac{\partial F}{\partial U}, \quad B = \frac{\partial G}{\partial U}$$

which should be satisfied in using the NND scheme (or other total variation diminishing (TVD) schemes). If the kinematic energy equation is not included, the above conditions cannot be satisfied. This is the reason to include the kinematic energy equation, although it is not independent and is not solved.

3. DISCRETE SCHEME

3.1. NND scheme

Consider the following model equation:

$$\frac{\partial u}{\partial t}+\frac{\partial f(u)}{\partial x}=0 \tag{10}$$

If $f(u)$ is a non-linear function of u, it is possible for Equation (10) to have a discontinuous solution. Most schemes will generate strong oscillations of solutions in the region around the discontinuity. To overcome this difficulty, the following scheme is used:

$$\begin{cases}\dfrac{u_j^{n+1}-u_j^n}{\Delta t}=-\dfrac{3f_j^{+n}-4f_{j-1}^{+n}+f_{j-2}^{+n}}{2\Delta x}-\dfrac{f_{j+1}^{-n}-f_{j-1}^{-n}}{2\Delta x}; & \text{upstream of discontinity}\\ \dfrac{u_j^{n+1}-u_j^n}{\Delta t}=\dfrac{3f_j^{-n}-4f_{j+1}^{-n}+f_{j+2}^{-n}}{2\Delta x}-\dfrac{f_{j+1}^{+n}-f_{j-1}^{+n}}{2\Delta x}; & \text{downstream of discontinity}\end{cases}$$

$$a=\frac{\mathrm{d}f}{\mathrm{d}u},\quad f=au,\qquad f^{\pm}=a^{\pm}u=\frac{a\pm|a|}{2}u$$

where j is the index of grid and n is the number of time levels. Δx is the scale of the grid, Δt is the time step. This scheme is commonly used to solve the above model equation (10). However, the computational result shows the following property: either scheme in upstream or downstream will generate numerical oscillation. In upstream of the discontinuity, the first scheme can force the numerical oscillation to propagate downward; on the other hand, the second scheme can force it upward. Therefore, the NND method combines these two schemes as follows: the first scheme is used upstream of discontinuity and second scheme is used downstream. Finally the numerical oscillation enters the trap and disappears.

Adding the criterion of discontinuity, the scheme has the following compact form:

$$\begin{cases}\dfrac{\partial u}{\partial t}=-\dfrac{1}{\Delta x}(h_{j+1/2}^n-h_{j-1/2}^n)\\ h_{j+1/2}^n=f_{j+1/2,\mathrm{L}}^n+f_{j+1/2,\mathrm{R}}^n\\ f_{j+1/2,\mathrm{L}}^n=f_j^{+n}+\dfrac{1}{2}\operatorname{minmod}(\Delta f_{j-1/2}^{+n},\Delta f_{j+1/2}^{+n})\\ f_{j+1/2,\mathrm{R}}^n=f_{j+1}^{-n}+\dfrac{1}{2}\operatorname{minmod}(\Delta f_{j+1/2}^{-n},\Delta f_{j+3/2}^{-n})\\ \operatorname{minmod}(a,b)=[\operatorname{sign}(x)+\operatorname{sign}(y)]\min(|x|,|y|)/2\\ \operatorname{sgn}(x)=\begin{cases}1 & x>0\\ 0 & x=0\\ -1 & x<0\end{cases},\quad \Delta f_{j+1/2}^{\pm n}=f_{j+1}^{\pm n}-f_j^{\pm n},\quad f^{\pm n}=\dfrac{f^n\pm|f^n|}{2}\end{cases} \tag{11}$$

The result of the computation shows that the scheme has no oscillation except at points where $\partial^2 u/\partial x^2 = 0$. Moreover, there is no free chosen parameter; hence the name the NND scheme. Generally the precision of the scheme is second-order, except when $f^{+n}_{j+1/2}$ and $f^{n}_{j-1/2}$ have different signs, i.e. minmod$(\cdot,\cdot) = 0$, the precision of the scheme reduces to first-order. Actually, the NND scheme is also a TVD scheme (see Appendix A).

3.2. One-dimensional

The surface of the Qiantangjiang tide varies widely. To avoid the pseudo-oscillation in the computation, we use the NND difference scheme.

Using the definition of F in Equation (3), we have

$$\begin{cases} \dfrac{\partial F}{\partial U} = \begin{pmatrix} 0 & 1 \\ -u^2 + \dfrac{gA}{B} & 2u \end{pmatrix} = L \begin{pmatrix} u + \sqrt{\dfrac{gA}{B}} & 0 \\ 0 & u - \sqrt{\dfrac{gA}{B}} \end{pmatrix} L^{-1} = L \begin{pmatrix} \lambda_1 & 0 \\ 0 & \lambda_2 \end{pmatrix} L^{-1} \\ \\ L = \begin{pmatrix} 1 & 1 \\ u + \sqrt{\dfrac{gA}{B}} & u - \sqrt{\dfrac{gA}{B}} \end{pmatrix}, \quad \lambda_{1,2} = u \pm \sqrt{\dfrac{gA}{B}} \end{cases} \tag{12}$$

Because $(\partial F/\partial U)U \neq F$, the NND scheme cannot be used directly. It is necessary to construct a matrix M, which has the same characteristic as that of $\partial F/\partial U$ and satisfies $MU = F$. M should be

$$M = \begin{pmatrix} u - \dfrac{AQ}{BI} & \dfrac{A^2}{BI} \\ \dfrac{gI}{A} - \dfrac{Q^2}{BI} & u + \dfrac{AQ}{BI} \end{pmatrix} = S \begin{pmatrix} \lambda_1 & 0 \\ 0 & \lambda_2 \end{pmatrix} S^{-1} = S \Lambda S^{-1} \tag{13}$$

$$S = \begin{pmatrix} \dfrac{IB}{2A^2} - \dfrac{u}{2}\sqrt{\dfrac{B}{gA}} & \dfrac{1}{2}\sqrt{\dfrac{B}{gA}} \\ \dfrac{IB}{2A^2} + \dfrac{u}{2}\sqrt{\dfrac{B}{gA}} & -\dfrac{1}{2}\sqrt{\dfrac{B}{gA}} \end{pmatrix} = \begin{pmatrix} S_{11} & S_{12} \\ S_{21} & S_{22} \end{pmatrix} \tag{14}$$

The characteristic decomposition of matrix M is

$$M = S\Lambda S^{-1} = S\Lambda^{+} S^{-1} + S\Lambda^{-} S^{-1} = M^{+} + M^{-}$$

$$F = MU = M^{+} U + M^{-} U = F^{+} + F^{-}, \qquad \Lambda^{\pm} = \frac{1}{2}(\Lambda \pm |\Lambda|) \tag{15}$$

Because the mesh is non-uniform and the transformation $x = x(\xi)$ is adopted, therefore

$$\frac{\partial F}{\partial x} = \frac{\partial F}{\partial \xi}\frac{\mathrm{d}\xi}{\mathrm{d}x} = \frac{F_{j+1/2} - F_{j-1/2}}{\Delta\xi}\frac{2\Delta\xi}{x_{j+1} - x_{j-1}} \tag{16}$$

Substituting the above relation into Equation (3) and using the NND difference scheme, we get

$$\frac{1}{\Delta t}(U_j^{n+1} - U_j^{n}) = -\frac{2}{x_{j+1} - x_{j-1}}(\mathrm{H}_{j+1/2}^{n} - \mathrm{H}_{j-1/2}^{n}) \tag{17}$$

where

$$\mathrm{H}_{j+1/2}^{n} = F_{j+1/2,\mathrm{L}}^{n} + F_{j+1/2,\mathrm{R}}^{n}$$

$$F_{j+1/2,\mathrm{L}}^{n} = F_j^{+n} + \frac{1}{2}\,\mathrm{minmod}[(F_j^{+n} - F_{j-1}^{+n}), (F_{j+1}^{+n} - F_j^{+n})]$$

$$F_{j+1/2,\mathrm{R}}^{n} = F_{j+1}^{-n} + \frac{1}{2}\,\mathrm{minmod}[(F_{j+1}^{-n} - F_j^{-n}), (F_{j+2}^{-n} - F_{j+1}^{-n})]$$

$$\mathrm{minmod}(x, y) = [\mathrm{sign}(x) + \mathrm{sign}(y)]\,\min(|x|, |y|)/2 \tag{18}$$

In the explicit scheme, the value of F in the nth time step in used. Equation (17) can be computed by time advancement. In the implicit scheme $F^{\pm} = M^{\pm n} U^{n+1}$, then Equation (17) constructs a set of equations that can be solved by using the column pivoting elimination method.

3.3. Two-dimensional

In the NND difference scheme the flux must be split

$$F_k = Fk_1 + Gk_2, \qquad P = Ak_1 + Bk_2, \qquad A = \frac{\partial F}{\partial U}, \qquad B = \frac{\partial G}{\partial U}, \qquad V_n = uk_1 + vk_2,$$

$$V_\tau = vk_1 - uk_2, \qquad V^2 = u^2 + v^2$$

where $\vec{k}$ is a vector normal to the side of an element, and k_1, k_2 are its two components. Then P can be split into $P = P^{+} + P^{-}$, where

$$P = Q\Lambda Q^{-1},$$

$$\lambda(P) = \{V_\tau + c\sqrt{k_1^2 + k_2^2},\ V_n,\ V_n,\ V_n - c\sqrt{k_1^2 + k_2^2}\}, \quad \Lambda = \{\lambda_1, \lambda_2, \lambda_3, \lambda_4\}$$

$$Q = \begin{pmatrix} 1 & 0 & 0 & 1 \\ u + n_1 c & v & n_2 & u - n_1 c \\ v + n_2 c & v & -n_1 & v - n_2 c \\ \dfrac{u^2+v^2}{2} + (n_1 u + n_2 v)c + c^2 & \dfrac{u^2+v^2}{2} & -n_1 v + n_2 u & \dfrac{u^2+v^2}{2} - (n_1 u + n_2 v)c + c^2 \end{pmatrix}$$

$$P^{\pm} = Q\Lambda^{\pm} Q^{-1} \tag{19}$$

where

$$n_1 = \frac{k_1}{\sqrt{k_1^2 + k_2^2}}, \quad n_2 = \frac{k_2}{\sqrt{k_1^2 + k_2^2}}, \quad \Lambda^{\pm} = \frac{1}{2}(\Lambda \pm |\Lambda|)$$

Then F can also be split into two parts, F_k^+ and F_k^-, $F_k^{\pm} = P^{\pm} U$

$$F_k^{\pm} = \frac{h}{4} \begin{pmatrix} \lambda_1^{\pm} + \lambda_2^{\pm} + \lambda_3^{\pm} + \lambda_4^{\pm} \\ \lambda_1^{\pm}(u + n_1 c) + (\lambda_2^{\pm} + \lambda_3^{\pm})u + \lambda_4^{\pm}(u - n_1 c) \\ \lambda_1^{\pm}(v + n_2 c) + (\lambda_2^{\pm} + \lambda_3^{\pm})v + \lambda_4^{\pm}(v - n_2 c) \\ \lambda_1^{\pm} \dfrac{(u + n_1 c)^2 + (v + n_2 c)^2 + c^2}{2} + (\lambda_2^{\pm} + \lambda_3^{\pm}) \dfrac{u^2 + v^2}{2} + \lambda_4^{\pm} \dfrac{(u - n_1 c)^2 + (v - n_2 c)^2 + c^2}{2} \end{pmatrix}$$

3.3.1. Explicit NND scheme. In the present paper, the NND scheme is extended to an unstructured grid system using ideas similar to the finite volume method. Here the velocity and height of the free surface of water are defined in the centre of the grid. Here all grids are triangles.

Integrating Equation (7) over each triangle element, we can obtain

$$\int_{\triangle ABS} \left(\frac{\partial U}{\partial t} + \frac{\partial F}{\partial x} + \frac{\partial G}{\partial y}\right) \mathrm{d}S = \frac{\partial U}{\partial t} \Delta S_i + \oint_{\triangle ABC} F_n \, \mathrm{d}l = \int_{\triangle ABC} H_i \, \mathrm{d}S \approx H_i \Delta S_i \tag{20}$$

where ΔS_i is area of the ith triangle element. In F_n, let $k_1 = n_1$, $k_2 = n_2$. In Equation (20), the right-hand second integral along the sides of the element can be calculated approximately as follows:

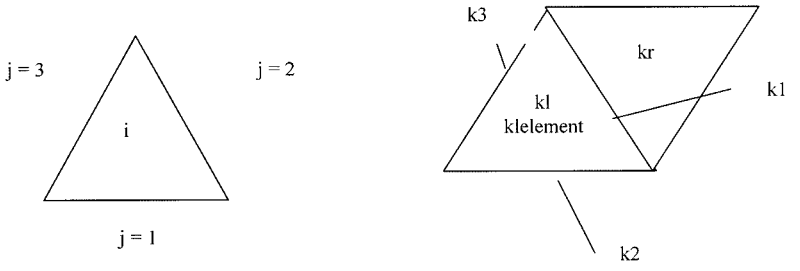

Sketch

$$\oint_{\triangle ABC} F_n \, \mathrm{d}l = \sum_{kb=1}^{3} F_n^{kb} \Delta L_{kb} = Q_b$$

where ΔL is the length of the element side, kb is $k1$, $k2$, $k3$. Discretizing the right first term in Equation (19) in time, the difference scheme is

$$\frac{U^{n+1} - U^n}{\Delta t} \Delta S_i + Q_{bi} = H_i \Delta S_i \tag{21}$$

It is clear that F_n have different values at the common side of two grid elements, so the flux passing the common side can be obtained by the Riemann solution. In the NND method, the flux can be calculated

$$\begin{aligned}
F_{nb} &= F_{n\mathrm{l}}^{+} + F_{n\mathrm{r}}^{-} \\
F_{n\mathrm{l}}^{+} &= F_{n,k\mathrm{l}}^{+} + \overline{\left(\frac{\partial F_n}{\partial x}\right)_{k\mathrm{l}}}^{+} \Delta x_{kb,k\mathrm{l}} + \overline{\left(\frac{\partial F_n}{\partial y}\right)_{k\mathrm{l}}}^{+} \Delta y_{kb,k\mathrm{l}} \\
F_{n\mathrm{r}}^{-} &= F_{n,k\mathrm{r}}^{-} + \overline{\left(\frac{\partial F_n}{\partial x}\right)_{k\mathrm{r}}}^{-} \Delta x_{kb,k\mathrm{r}} + \overline{\left(\frac{\partial F_n}{\partial y}\right)_{k\mathrm{r}}}^{-} \Delta y_{kb,k\mathrm{r}}
\end{aligned} \tag{22}$$

where

$$\begin{aligned}
\overline{\left(\frac{\partial F_n}{\partial x}\right)_{k\mathrm{l}}}^{+} &= \mathrm{minmod}\left[\left(\frac{\partial F_n^{+}}{\partial x}\right)_{k\mathrm{l}}, \left(\frac{\partial F_n^{+}}{\partial x}\right)_{k\mathrm{r}}\right] \\
\overline{\left(\frac{\partial F_n}{\partial x}\right)_{k\mathrm{l}}}^{-} &= \mathrm{minmod}\left[\left(\frac{\partial F_n^{-}}{\partial x}\right)_{k\mathrm{l}}, \left(\frac{\partial F_n^{-}}{\partial x}\right)_{k\mathrm{r}}\right] \\
\overline{\left(\frac{\partial F_n}{\partial y}\right)_{k\mathrm{l}}}^{+} &= \mathrm{minmod}\left[\left(\frac{\partial F_n^{+}}{\partial y}\right)_{k\mathrm{l}}, \left(\frac{\partial F_n^{+}}{\partial y}\right)_{k\mathrm{r}}\right] \\
\overline{\left(\frac{\partial F_n}{\partial y}\right)_{k\mathrm{l}}}^{-} &= \mathrm{minmod}\left[\left(\frac{\partial F_n^{-}}{\partial y}\right)_{k\mathrm{l}}, \left(\frac{\partial F_n^{-}}{\partial y}\right)_{k\mathrm{r}}\right]
\end{aligned} \tag{23}$$

$$\text{minmod}(a, b) = [\text{sign}(a) + \text{sign}(b)] \min(|a|, |b|)/2$$

$$\Delta x_{kb,k\text{l}} = x_{kb} - x_{k\text{l}}, \qquad \Delta y_{kb,k\text{l}} = y_{kb} - y_{k\text{l}}$$

$$\Delta x_{kb,k\text{r}} = x_{kb} - x_{k\text{r}}, \qquad \Delta y_{kb,k\text{r}} = y_{kb} - y_{k\text{r}} \tag{24}$$

The subscript kb denotes a side of the kth element, which can be $k1$, $k2$ or $k3$. $k\text{l}$ and $k\text{r}$ denote elements on the left and right side of kb respectively.

3.3.2. Calculation of the first derivative. In the above mentioned difference scheme, there are gradients of flux F_n that must be calculated. Numerical results show the great influence of the methods to determine the flux gradient. There are many methods to determine it. Here we use the least-squares method. In this method, the Taylor series is used

$$e\varphi_j = \varphi_i + \frac{\partial \varphi_i}{\partial x}(x_j - x_i) + \frac{\partial \varphi_i}{\partial y}(y_j - y_i) \quad (j = 1, 2, 3) \tag{25}$$

Here $e\varphi_j$ is the calculated value of φ at the centre of neighbour element j. The high-order small values are ignored. Using this equation, we can get the following function:

$$f\left(\frac{\partial \varphi_i}{\partial x}, \frac{\partial \varphi_i}{\partial y}\right) = \sum_{j=1}^{3} (e\varphi_j - \varphi_j)^2 \tag{26}$$

where φ_j is the real value at the centre of the neighbour element j. By minimizing the value of f, we can get the optimal values of the gradients:

$$\frac{\partial \varphi_i}{\partial x} = \frac{\sum_{j=1}^{3} \{[(x_j - x_i)r_{22} - (y_j - y_i)r_{12}](e\varphi_j - \varphi_i)\}}{r_{11}r_{22} - r_{12}^2}$$

$$\frac{\partial \varphi_i}{\partial y} = \frac{\sum_{j=1}^{3} \{[(y_j - y_i)r_{11} - (x_j - x_i)r_{12}](e\varphi_j - \varphi_i)\}}{r_{11}r_{22} - r_{12}^2} \tag{27}$$

where

$$r_{11} = \sum_{j=1}^{3} (x_j - x_i)^2; \quad r_{22} = \sum_{j=1}^{3} (y_j - y_i)^2; \quad r_{12} = \sum_{j=1}^{3} (x_j - x_i)(y_j - y_i)$$

In this method, the gradients of variables are determined by using only the value in the element and the three values in its neighbouring elements. When the ith element is near the wall boundary and one of its neighbouring elements is out of the domain, we set up a mirror triangle around the wall boundary. The variables' values in the mirror element are determined by the mirror method, thus the above equations can be used. When the ith element is near the water boundary and one of its neighbouring elements is out of the domain, and the central

point of the triangle is replaced by the mid-point of the side on the water boundary, the variables values can be determined easily.

Here the variable φ can be replaced by h, u, v, $F_n^{\pm}$, then their gradients can be determined.

4. BOUNDARY CONDITION

4.1. One-dimensional problem

By the above discussion we know that the values at the three points are used to calculate values at an inner point. These three points are the inner point and its two neighbouring points. Therefore, the values of boundary points and near-boundary points must be determined using the boundary condition. In the present computation, the characteristic method is used. Using characteristic analysis, the characteristic relations are

$$-(\lambda_1+\lambda_2-\lambda)\,\mathrm{d}A+\mathrm{d}Q=e\,\mathrm{d}t,\quad e=-gA\zeta(x,t)+g\frac{A}{B}A_x(x,t)-gAS_f \tag{28}$$

Upstream, the flux $Q(t)$ is given. Downstream, the water level $\zeta(t)$, which is equivalent to $A(t)$, is given. Upstream, $\lambda_1>0$, $\lambda_2<0$, so the direction of the first group characteristic line is inward while the direction of the second group characteristic line is outward. The relation on the first group characteristic line is substituted by the boundary condition and we only need the relation on the second group characteristic line. In Figure 4, AP is the second group characteristic line and the relation on it after discretion is

$$A_A=A_P+\frac{1}{\lambda_M}(Q_A-Q_P-e_M\Delta t) \tag{29}$$

where λ_M is the characteristics value at point M.

Constructing a quadratic function by the values of points 1, 2, 3, the value of point P and the derivative value of the boundary point are obtained by interpolation. The value at point B, which is near the boundary, is obtained by the relation between the two characteristic lines. The calculation of the right boundary point is similar.

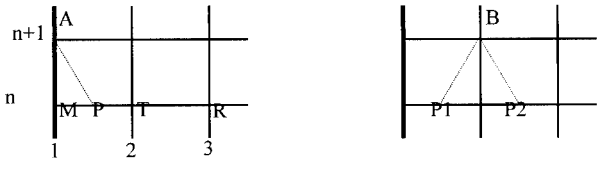

Figure 4. Calculation at left boundary point.

4.2. Two-dimensional problem

The stability and precision of computation are directly influenced by the boundary conditions (see Reference [20]), especially in the computation of the unstructured grid. It is more difficult because of the irregularity of the grid. From the characteristic theory of two-dimensional unsteady flow, we know that there are characteristic cones in the x-, y-, t-directions. There are infinite consistent relations, which are very complex. In the water boundary, the cross-line of the characteristic cone and $t =$ constant plane is an ellipse, which is located partly in the domain and partly out of the domain, or entirely in/out of the domain, so that it is not easy to use the characteristic consistent relation. In the present paper, the characteristic condition is simplified and the boundary condition is dealt with by a one-dimensional local characteristic method and a non-reflective method.

In the present paper, boundary conditions are divided into three parts: wall boundary, water boundaries and moving boundary. The water boundaries are divided into upstream and downstream boundaries. The boundary conditions on the different boundaries are discussed below.

4.2.1. Wall boundary condition. The component of the velocity in the normal direction on the wall equals zero

$$\vec{V} \cdot \vec{n} = 0 \tag{30}$$

Since the viscosity is not considered, the tangential component velocity is not equal to zero.

4.2.2. Water boundary condition at upstream and downstream. Usually the water level or discharge (e.g. velocity) at upstream or downstream can be measured. According to the characteristic line theory, we can calculate the flow velocity on the water boundary according to the water level, or the water level according to the discharge. That is a quasi-one-dimensional approximation on the upstream and downstream boundary. The one-dimensional local characteristic line method and the non-reflective boundary condition are given as follows:

(a) **Characteristic line method**

The one-dimensional characteristic relation is used in the treatment of upstream and downstream boundaries.

One-dimensional unsteady shallow water equations are

$$\frac{\partial U}{\partial t} + \frac{\partial F}{\partial x} = H \tag{31}$$

where

$$U = \begin{pmatrix} h \\ hu \end{pmatrix}; \qquad F = \begin{pmatrix} hu \\ hu^2 + hc^2/2 \end{pmatrix}; \qquad H = \begin{pmatrix} 0 \\ h_2 \end{pmatrix}, \quad h_2 = gh(S_x - S_{fx})$$

Let

$$A = \frac{\partial F}{\partial U} = \begin{pmatrix} 0 & 1 \\ -u^2 + c^2 & 2u \end{pmatrix} \tag{32}$$

We obtain eigenvalues and the left eigenvector of A

$$\lambda(A) = (u + c, u - c), \qquad X = \begin{pmatrix} \lambda - 2u \\ 1 \end{pmatrix} \tag{33}$$

According to characteristic line theory, the consistency relations on the characteristic lines can be expressed as follows:

$$X \cdot \left(\frac{\partial U}{\partial t} + A \frac{\partial U}{\partial x} - H \right) = 0 \tag{34}$$

namely

$$(\lambda - u) \frac{\partial h}{\partial t} + h \frac{\partial u}{\partial t} + (-u^2 + c^2 + \lambda u) \frac{\partial h}{\partial x} + \lambda h \frac{\partial u}{\partial x} = h_2 \tag{35}$$

When $\lambda = u + c$, Equation (34) is simplified as follows:

$$c \left[\frac{\partial h}{\partial t} + (u + c) \frac{\partial h}{\partial x} \right] + h \left[\frac{\partial u}{\partial t} + (u + c) \frac{\partial u}{\partial x} \right] = h_2 \tag{36}$$

and when $\lambda = u - c$, Equation (35) is simplified as follows:

$$-c \left[\frac{\partial h}{\partial t} + (u - c) \frac{\partial h}{\partial x} \right] + h \left[\frac{\partial u}{\partial t} + (u - c) \frac{\partial u}{\partial x} \right] = h_2 \tag{37}$$

These are the characteristic relations on the one-dimensional characteristic lines.

In this paper, we choose the water boundary whose normal direction is parallel to the velocity vector. It is easily satisfied in the narrow river but is difficult in the downstream, where the water region is wide and the direction of real flow is unsteady. However, the averaged direction on the downstream is determined according to the observation data in Figure 5. In Figure 5, we choose a tide difference isoline near Ganpu as the downstream boundary, and once this line is determined we can deal with the boundary condition by using the one-dimensional local characteristic line method.

Because the normal directions of boundary lines at upstream and downstream are parallel with the x'-direction, which is obtained by rotating the original co-ordinates x–y, then the characteristic relation in x' is used.

The values on the boundary are defined at the vertex of triangles. In Figure 6(a), $\triangle ABC$ is a boundary triangle, BC is on the boundary and B and C have values. Here it is assumed that the values between BC are linearly distributed and the values at points on this line segment are expressed by the values at points B and C. In Figure 6, i is the mid-point of the triangle, iD is a line segment passing point i and is normal to BC, its length is Δl and D is pedal. Figure 6(a) is an x–y plane figure and Figure 6(b) is an x'–t plane figure. iP is an outward characteristic line that intersects with the t-axis at point E, and point D is at the nth time level. The time step is dt and the length of ED is Δt. According to the characteristic relation discussed above, we obtain

$$c\frac{h_E - h_i^n}{\Delta t} + h\frac{V_{nE} - V_{ni}^n}{\Delta t} = h_2 \tag{38}$$

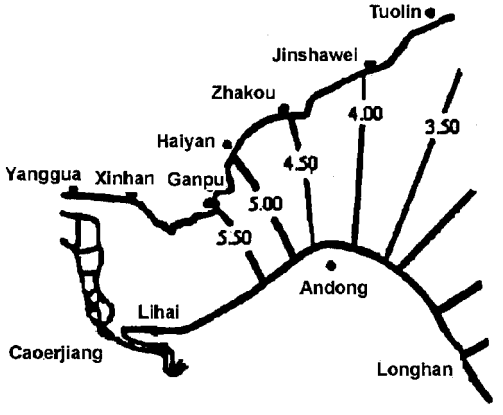

Figure 5. Contours of average tide difference.

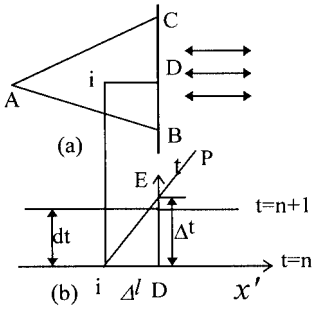

Figure 6. Sketch of characteristic method.

where $\Delta t = \Delta l/(V_n + c)$. The values of c, h, V_n are taken in the central point of $\triangle ABC$ by explicit form, thus only V_{nE} is unknown in the above equation. By using the following equation:

$$V_{nE} = \frac{h_2 \Delta t - c_i^n (h_E - h_i^n)}{h_i^n} + V_{ni}^n \tag{39}$$

we obtain the value of V_{nE} on $t = n$. We solve the value of V_n on $t = n + 1$ by interpolation

$$V_{nD}^{n+1} = \frac{\mathrm{d}t}{\Delta t} (V_{nE} - V_{nD}^n) + V_{nD}^n \tag{40}$$

Here only the characteristic line of $\lambda = V_n + c$ is used. When $|V_n| < c$ (slow flow) on the open boundary of upstream and downstream, there always is $V_n + c > 0$ and its corresponding characteristic line iP always intersects with the boundary. When $V_n < -c$ (rapid flow) on the open boundary of upstream and downstream, the relation should be changed into the consistency relation corresponding to eigenvlaue $V_n - c$. In the computation process of the Qiantangjiang tide, the downstream surface is wide and hence $|V_n| < c$. There is rapid flow at upstream with floods and $V_n > 0$, so $V_n + c > 0$. Because x' is the normal direction of the boundary line, the above results are applicable for upstream and downstream boundaries, but the original co-ordinate system must be rotated before using the quasi-one-dimensional characteristic relation.

When the values of velocity at every time step are known, Equation (38) can also be used to determine the water level at the $(n + 1)$th time step by the velocity and water level at the nth time step

$$h_E = \frac{h_2 \Delta t - h(V_{nE} - V_{ni}^n)}{c + h_i^n} \tag{41}$$

$$h_D^{n+1} = \frac{\mathrm{d}t}{\Delta t} (h_E - h_D^n) + h_D^n \tag{42}$$

In order to guarantee stable condition, $\mathrm{d}t < \Delta t$ must be satisfied. Hence, when the grid is very dense the time step must be very small.

(b) **Non-reflective boundary condition**

The water boundary at upstream is located at a straight part of the river, so we can assume that there is no reflected wave back to the domain, i.e. the outer region has no influence on the computational domain. When the tide ebbs, the upstream wave moves inward and the water surface is gentle, and we can assume the conditions are satisfied [20]; at the boundary, the amplitude of the incidence wave does not vary with time. This is a non-reflective boundary condition, corresponding to the characteristic lines of the inward and outward waves, so that we can obtain two equations.

For the outward characteristic line corresponding to $\lambda = V_n + c$, there is an expression similar to characteristic relation (37)

$$(c - V_n)\frac{\partial h}{\partial t} + \frac{\partial (hV_n)}{\partial t} = h_2 + (V_n^2 - c^2)\frac{\partial h}{\partial x'} - (V_n + c)\frac{\partial (hV_n)}{\partial x'} \tag{43}$$

For the inward characteristic line $\lambda = V_n - c$, according to the assumption that the wave amplitude is invariable, in the corresponding characteristic relation, the derivative $\partial/\partial x' = 0$, i.e.

$$(-c - V_n)\frac{\partial h}{\partial t} + \frac{\partial (hV_n)}{\partial t} = 0 \tag{44}$$

Using the above two equations we get

$$\frac{\partial h}{\partial t} = -\frac{V_n + c}{2c}\left(h\frac{\partial V_n}{\partial x'} + c\frac{\partial h}{\partial x'}\right) + \frac{h_2}{2c} \tag{45}$$

$$\frac{\partial (hV_n)}{\partial t} = (c + V_n)\frac{\partial h}{\partial t} \tag{46}$$

On the right-hand side of Equation (45) there is no temporal derivative. Using the values of h in the nth step, the distributions of V_n and c can be obtained and $\partial h/\partial t$ on the left-hand side of the equation can also be obtained. From Figure 6, the discrete form of Equation (45) is

$$\frac{h_D^{n+1} - h_D^n}{\mathrm{d}t} = -\frac{V_{ni}^n + c_i^n}{2c_i^n}\left(h_i^n\frac{V_{nD}^n - V_{ni}^n}{\Delta l} + c_i^n\frac{h_D^n - h_i^n}{\Delta l}\right) + \frac{h_2}{2c_i^n} \tag{47}$$

$\partial (hV_n)/\partial t$ is obtained by substituting $\partial h/\partial t$ into the right-hand side of Equation (46) and its discrete form is

$$\frac{(hV_n)_D^{n+1} - (hV_n)_D^n}{\mathrm{d}t} = (c + V_n)\frac{h_D^{n+1} - h_D^n}{\mathrm{d}t} \tag{48}$$

In this way, the values in the $(n+1)$th stratum are directly deduced from the values in the nth stratum and do not need the temporal interpolation, which is required in the characteristic line method. It is worthwhile to supplement here that the signs are unanimous with the characteristic line method and the discretion of Equations (47) and (48) is done in the boundary triangle of Figure 6(a). Despite presuming that there is no tangential velocity in the upstream or downstream, we do not assume that the normal velocity is congruent, the results are local and the computation must be done for every triangle on the boundary. Regardless of whether the characteristic line method or non-reflective boundary condition is used, the final goal is to deduce the boundary values at the $t = n + 1$ stratum from the values at the $t = n$ stratum.

(c) **Moving boundary**

The topograph of the estuary has a great variance and there is a shoal and island in the river. In the movement process of the Qiangtangjiang tide, these areas will come out at ebb and will

be submerged at flood time. In fact, it is a problem with the moving boundary. For problems with moving boundaries, the method, which is similar to the method in Reference [9], is adopted. It is assumed that there is a thin water layer δ in the computation area, which avoids the problem with moving boundary. In the computation, the following criterion is adopted in order to avoid that the layer in the non-water area becomes too thin, which would ruin the computation

$$\begin{cases} h_i^{n+1} = h_i^{\text{new}}, & h_i^{\text{new}} \geq 5\delta \\ h_i^{n+1} = \delta, & h_i^{\text{new}} < 5\delta \end{cases} \tag{49}$$

To check the correctness of the method, the example given by Hall and Watts [21] is used to simulate a climb of a soliton wave on a slope and is compared with Hall and Watts' [21] data.

5. NUMERICAL SIMULATION OF ONE DIMENSION

In this and the next section, numerical results will be presented. Because of the geometrical complexity of the Qiantangjiang river and the Hangzhou Gulf, as well as the difficulty of getting the observation data, there are few data to compare with the results of the numerical simulation. Therefore, to prove the correctness and reliability of the present method, some prototype examples are simulated and their results are compared with respective theoretical analysis and measurement data.

In the one-dimensional simulation of tide in the Qiantangjiang river, an adaptive mesh is adopted. The mesh in the computation is varied, i.e. is finer in the region with rapid variance of water level and coarse in that with slower variance of the water level. Therefore, the mesh must be adjusted at every time step. Here, a parameter

$$c_j = 1 + \alpha \left| \frac{\partial \zeta}{\partial x_j} \right| \tag{50}$$

and an energy function

$$E = \sum_j \frac{1}{2} c_j (x_j - x_{j-1})^2$$

are introduced. The values x_j ($j = 2, 3, \ldots, J-1$) are determined to minimize E. It is an adaptive procedure. The degree of adaptiveness can be adjusted according to the value of α.

5.1. Problem with exact solution

To check the correctedness of the above numerical method, this method is used to solve a problem with an exact solution. Let the riverbed be horizontal and the river width b be constant, and the Chezy coefficient C be constant too. Let $u > 0$. It is assumed that the

solution of Equations (1) and (2) are functions of $x - Vt$, where V is a constant. Then these two equations reduce to the following form:

$$h(V-u) = C_1 = \text{constant}$$

$$-V(hu)' + 2u(hu)' + ghh' = u^2h' - \frac{g}{C^2}u^2 \tag{51}$$

where the prime denotes the derivative with respect to $x - Vt$. From the above two equations, the solution can be obtained by

$$u' = \frac{gu^2}{C^2\left[C_1 - C_1^2\dfrac{g}{(u-V)^3}\right]} \tag{52}$$

Integrating Equation (3), the following formula is obtained:

$$\left\{\frac{C_1}{u} + C_1^2 g\left[\frac{1}{uV^3(u-V)^2}\left(V^2 - \frac{9}{2}uV + 3u^2\right) + \frac{3}{V^4}\ln\left(\frac{V}{u} - 1\right)\right]\right\}_{\theta_0}^{\theta} = \frac{g}{C^2}(\theta - \theta_0) \tag{53}$$

where

$$h = \frac{C_1}{V-u}, \qquad \theta = x - Vt \quad \text{and} \quad C_1 = h(u-V)$$

Here we consider $V = 5\ \text{m s}^{-1}$, $C = 1000\ \text{m}^{1/2}\,\text{s}^{-1}$, $C_1 = 20\ \text{m}^2\,\text{s}^{-1}$ and $z_b = 4$ m. The function $u(\theta)$ is determined by means of the computation of θ according to the given value of u. In this example, u varies from 2.5 to 4.0, x locates the region (0, 50972 m), the number of meshes is 151, the average scalar of mesh is $\Delta x = 340$, $\mathrm{d}t = 15$, and parameter $\alpha = 1000$. In Figures 7 and 8, the water level is plotted as a function of $x - Vt$ and the numerical result is almost the same as the exact solution. It means that the computation is stable and exact. Because the difference between the exact solution and the numerical solution is very small, the curves of both solutions are identical to each other and cannot be distinguished graphically.

5.2. Numerical simulation of water jump

The water jump is a typical non-linear water wave motion. When the width of a straight channel is constant and its bed is horizontal, the wave jump will propagate with a constant speed and shape. As in Figure 9, water jump moves from left to right with speed V, where the water depth in upstream is h, velocity is u and discharge is Q. In downstream, the velocity is $u_1 = 0$ and the water depth is h_1, the solution of the water jump is known

$$V = \sqrt{\frac{gh}{2h_1}(h + h_1)}$$

$$Q = Vb(h - h_1)$$

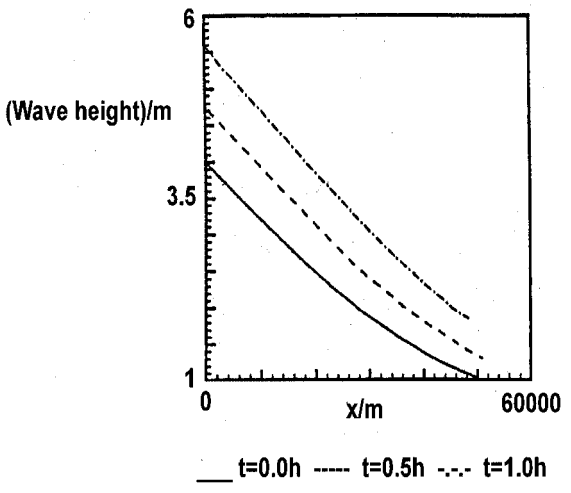

Figure 7. Water surface levels at three times.

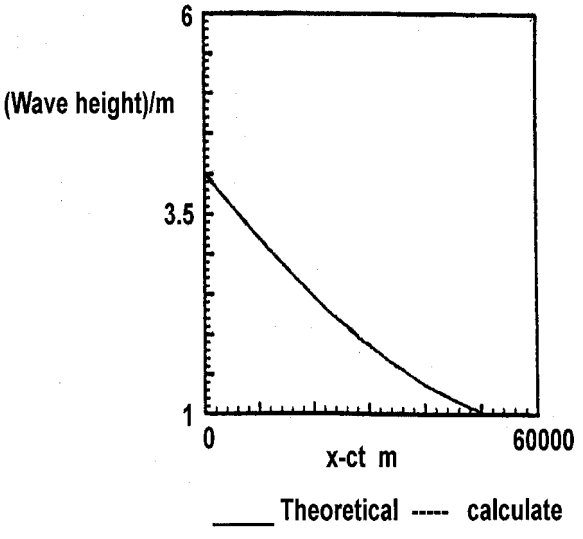

Figure 8. Two-lines in Figure 7 are shifted to the third line.

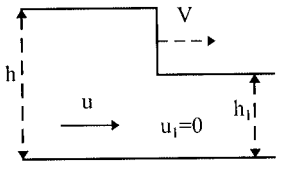

Figure 9. Sketch of water jump.

$$u = V\left(1 - \frac{h_1}{h}\right) \tag{54}$$

In the present computation with $x \in (0, 40\,696.8\ \text{m})$, the initial position of the water jump is close to x = 20250.9 m. For the computation, we use $h = 8$ m, $h_1 = 6$ m and $z = -4$ m. The computational result is $V = 9.56870\ \text{m s}^{-1}$, in which the number of meshes is 641 and $\mathrm{d}t = 0.5$. Figure 10 gives the comparison between the computational and theoretical solutions. In this case, the adapted grid (see Equation (50)) is used. Therefore, the dense grids are used around the jump and move with the jump. In other one-dimensional cases with discontinuity, this method is used too. In Figure 10 the solid line denotes theoretical results and it is covered over by calculated results; therefore the jump is not displayed clearly in the figure. When the uniform grid system is used, the solution is smeared and the jump cannot be displayed, then it is not compared with theoretical results in Figure 10.

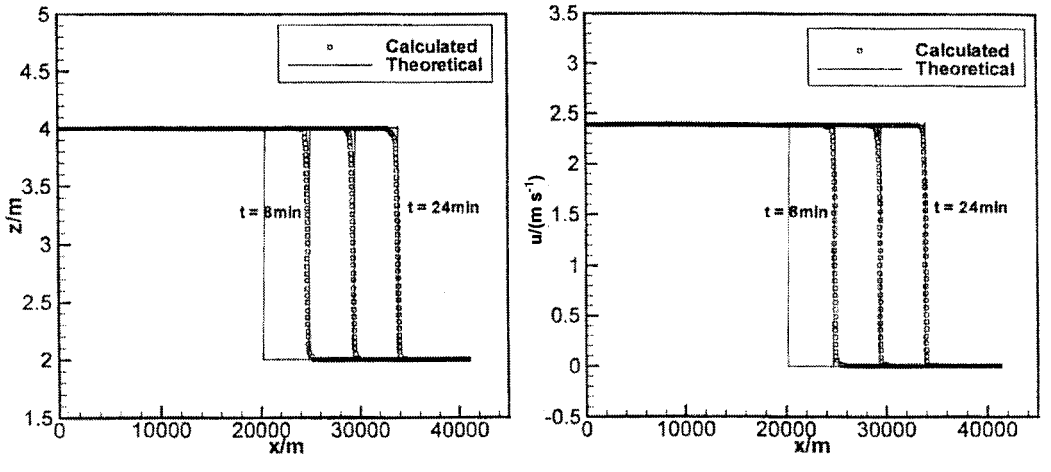

Figure 10. Comparison between computational results and theoretical solution of moving water jump.

5.3. Numerical simulation of dam-break

Suppose there is a channel with constant width and a horizontal bed. In the channel the water is separated into two parts with a dam. The water depths are h_1 on the left part and h_4 at the right part, where $h_4 > h_1$ (Figure 11). When $t < 0$, it is assumed that the water is static. At $t = 0$, the dam breaks suddenly, the water wave will propagate to left and right directions and the whole region is divided into four domains (see Figure 12). Domains 1 and 2 are separated by a discontinuity section that propagates leftward with velocity V. The free water surfaces are horizontal in domains 1, 2 and 4, and is a parabola in domain 3. The shapes and water levels can be calculated with the following theoretical formulas (see Figure 13). The initial situation of the dam is

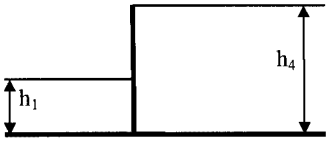

Figure 11. Initial situation of dam.

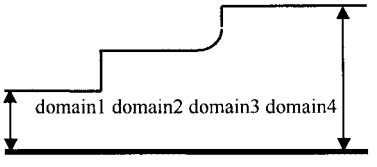

Figure 12. Later situation of dam.

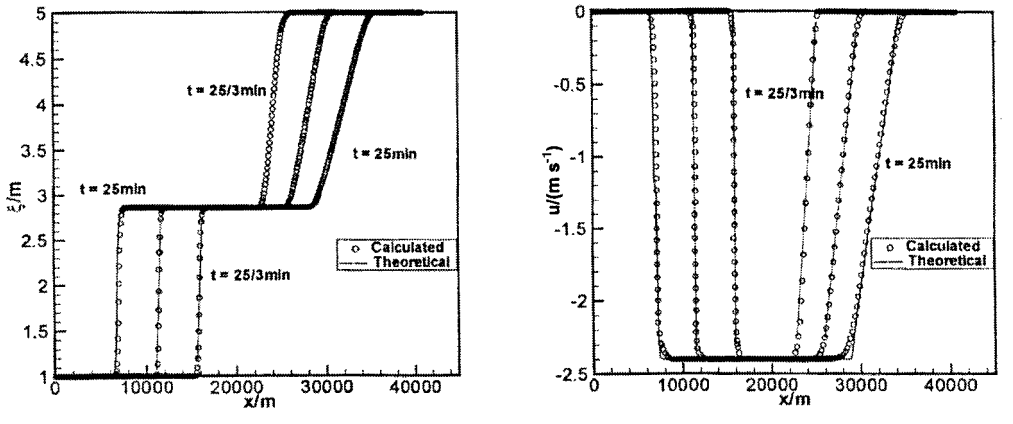

Figure 13. Comparison between computational results and theoretical solution of dam break.

$$\begin{cases} \dfrac{u_2}{C_1} = \dfrac{V}{C_1} - \dfrac{C_1}{4V}\left[1 + \sqrt{1 + 8\left(\dfrac{V}{C_1}\right)^2}\right] \\ \dfrac{C_2}{C_1} = \sqrt{\dfrac{1}{2}\left(\sqrt{1 + 8\left(\dfrac{V}{C_1}\right)^2} - 1\right)} \\ 2C_2 - u_2 = 2C_4 \end{cases} \tag{55}$$

where $C_i = \sqrt{gh_i}$, $i = 1, 2, 4$, h_i is water depth of area i. The water depth of domain 3 is as follows:

$$gh_4 = \frac{1}{9}\left(2C_4 + \frac{x - x_0}{t}\right)^2$$

where x_0 is the initial position of the dam. Here $h_1 = 5$ m, $h_4 = 9$ m, and hence $C_1 = 7.0036$, $C_4 = 9.3963$. Let $\varphi = V/C_1$. The above equations (55) can be rewritten in the following form:

$$\left\{\frac{1}{4\varphi}\left[1 + \sqrt{1 + 8\varphi^2}\right] - \varphi + 2.6833\right\}^2 = 2\sqrt{1 + 8\varphi^2} - 2 \tag{56}$$

From Equation (56) we can obtain $\varphi = 1.273$. Then the flow field in all the areas can be determined: $u_2 = -2.4$ m s^{-1}, $h_2 = 6.848$ m and $V = -8.916$ m s^{-1}.

Figure 13 displays the result with the above-mentioned numerical method of dam-break. In this figure $t = 0$, 500, 1000, 1500 s. The computational region is from $x = 0$ to x = 40696.8 m and the initial dam is located at $x_0 = 20250.9$ m. The riverbed locates at z = -4 m, hence the water levels in both sides of dam in Figure 13 are 1 and 5 m respectively. The number of meshes is $J = 641$ and d$t = 0.5$. The numerical computational results show good agreement with theoretical results. It indicates that the numerical method is applicable to compute flow with discontinuity providing the mesh is fine enough to catch the discontinuous surface. In this case, the adapted grid is used.

5.4. Numerical results of the Qiantangjiang tide

In the present computation, the initial time is 06:00 h, 25 August 1991. The upstream locates at Fuchunjiang power station where discharge Q is given. The downstream locates at Ganpu where water level ζ is given. These are periodic functions of time. The initial flow can be arbitrary, because its influence will be eliminated after some periods. The length of the computational domain is 194 km, the number of meshes is $J = 801$, the average mesh length is d$x = 243$ m. In this computation, the adjust parameter $\alpha = 1000$, the minimum scale of mesh dx is 13.1 m and its maximum is 257.8 m. Figure 14 shows the water level h and the corresponding dx via x. It is clear that the large dx corresponds to the small derivative d$h(x)$/dx and the small dx to the large derivative. In this computation, the semi-implicit scheme is used and the time step is d$t = 12$ s.

There are four tributaries at x = 42250, 62700, 70100, 79300 m, $x = 0$ is the initial point of upstream (Fuchunjiang power station) and downstream $x = 194000$ at Ganpu (see Figure 1). The computational result shows that the flux in the tidal inlet is lower than that without the

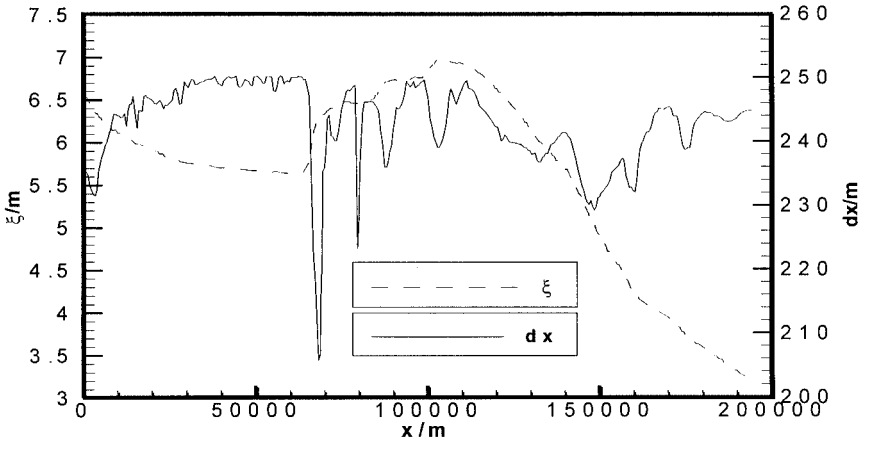

Figure 14. Wave shape via mesh.

influences from the tributaries. In order to obtain the correct discharge, the discharge parameters of tributaries are $\varepsilon^- = 0.2$, $\varepsilon^+ = 0$. For simplification, it is assumed that the tributaries are normal to the main flow, i.e. $u' = 0$.

There are six observation stations between the upstream boundary (Fuchunjiang power station) and the downtream boundary (Ganpu). Figures 15–20 compare the numerical and

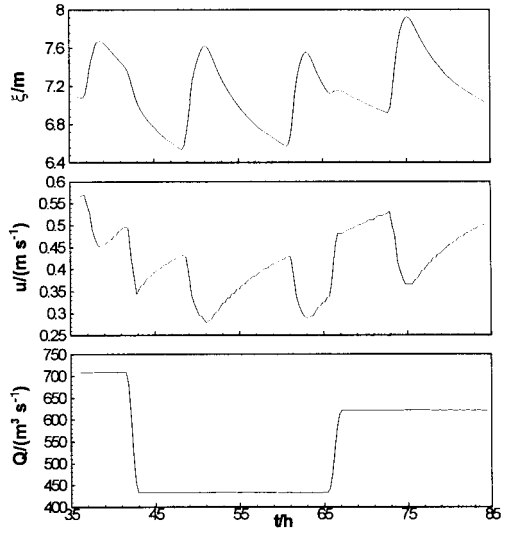

Figure 15. Data at Fuchunjiang power station.

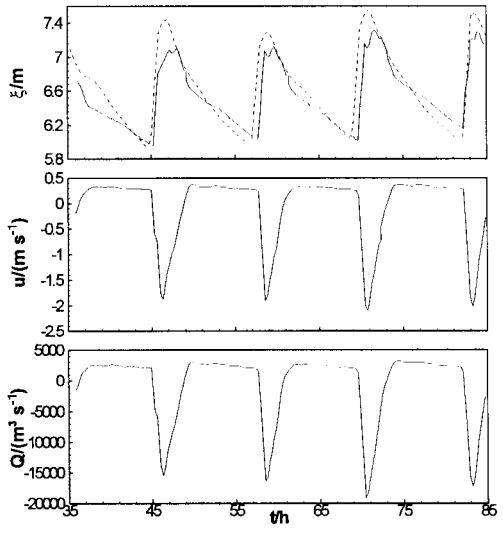

Figure 16. Data at Wenjiayan.

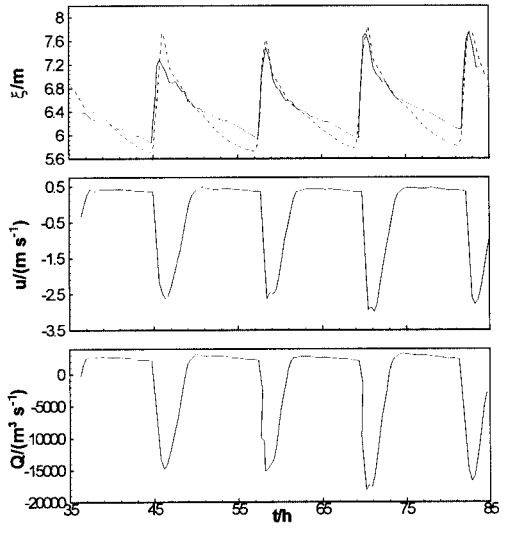

Figure 17. Data of Zhakou.

observed results at six stations, namely Fuchunjiang power station, Wenjiayan, Zhakou, Qibao, Yanguan and Ganpu. The small circles (Figure 19) or dash lines (Figures 16–18) denote the observed results and the solid lines denote the computational results. In the

computation, the total time is 85 h but only the results in the last 49 h are displayed in these figures. From these results, we can find that the differences between the computational and observed peak and valley values of the tide are less than 0.2 m at the stations. In Figure 21,

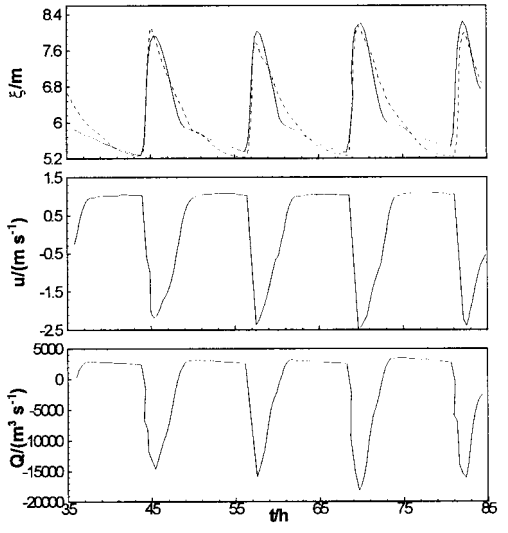

Figure 18. Data of Qibao.

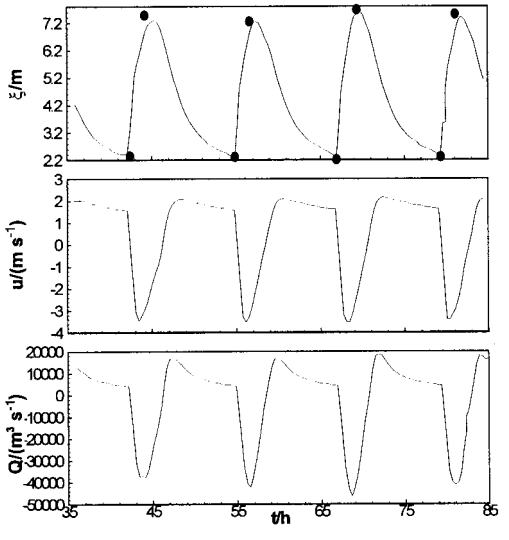

Figure 19. Data at Yanguan.

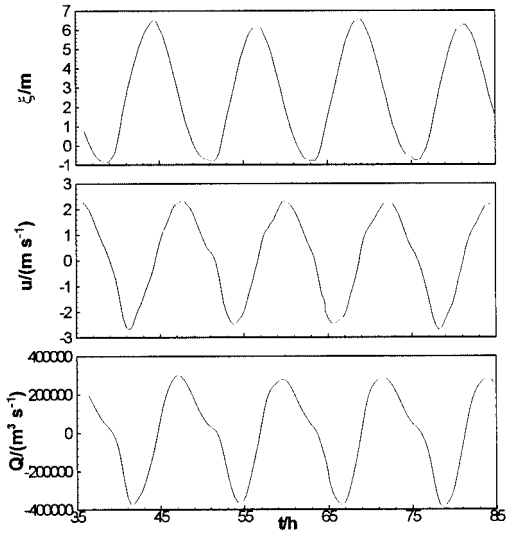

Figure 20. Data at Ganpu.

the wave level $\zeta(x)$ at $t = 62, 64, \ldots, 84$ are shown. The evolution of the tide in the river is displayed clearly.

6. NUMERICAL SIMULATION OF TWO DIMENSION

6.1. Simplified dam-break problem

The reason for choosing the NND scheme is that this scheme can catch strong continuity in flow. This numerical example is used to verify this ability of the NND scheme in the numerical simulation of shallow water problems. As we know, this problem can be exactly solved with the Riemann method. The numerical result can be compared with its exact solution and its efficiency will be examined. In this example, the friction on the bottom is ignored and the bottom is a horizontal plane. The initial water level is

$$h = \begin{cases} 9.0 & x > 70 \\ 5.0 & x \leq 70 \end{cases} \tag{57}$$

The grid system is shown in Figure 22. Using the NND scheme, the numerical result is displayed in Figures 23 and 24. Clearly the agreement between them is very good and there is no pseudo-oscillation in the numerical solution. It should be pointed out that the least-squares method is used to calculate the first-order derivatives of functions, such as velocity and flux.

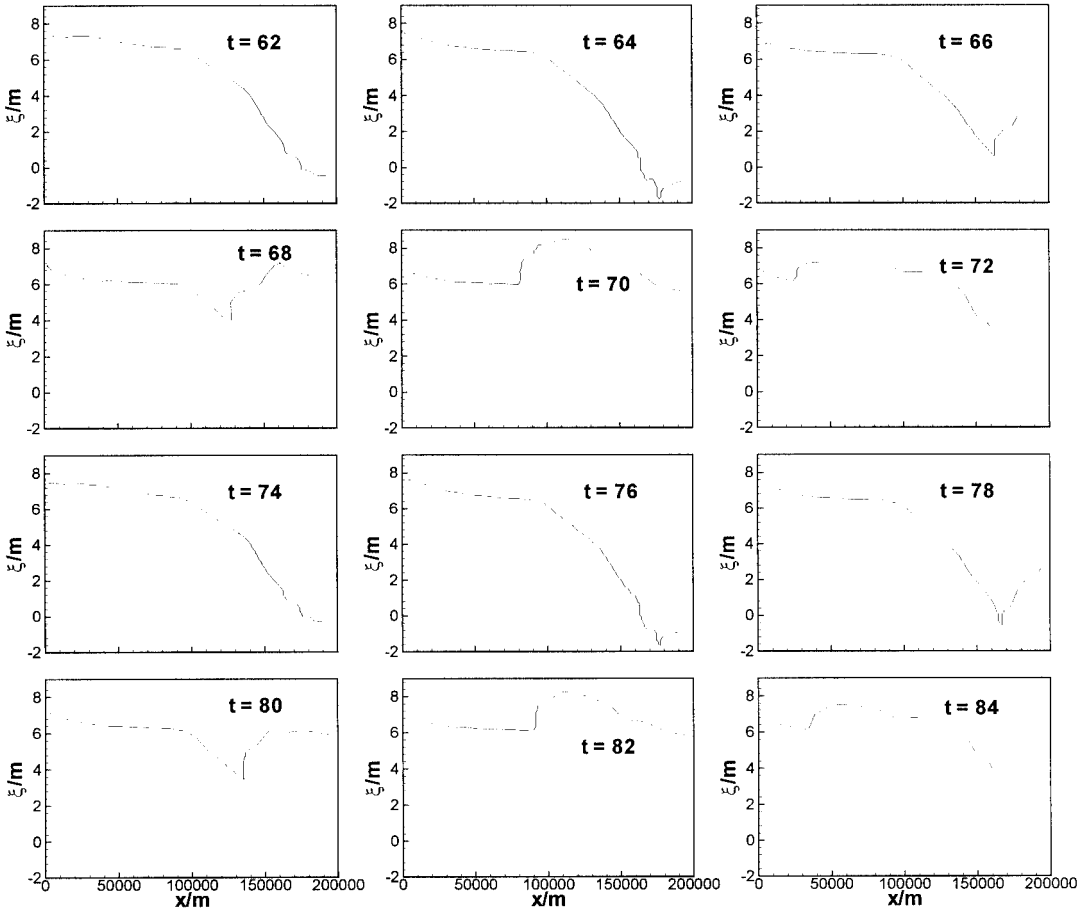

Figure 21. water level along river at different moments.

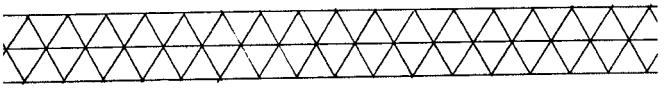

Figure 22. Grid system.

6.2. Dam-break problem in curve channel

Miller and Chaudry [22] constructed an experiment of a dam-break flow in a curved channel. In their paper, the details of their experimental equipment and result were provided. We select this problem as a test problem in this paper. Figures 25 and 26 display the sketch chart of the experimental equipment and the unstructured grid system.

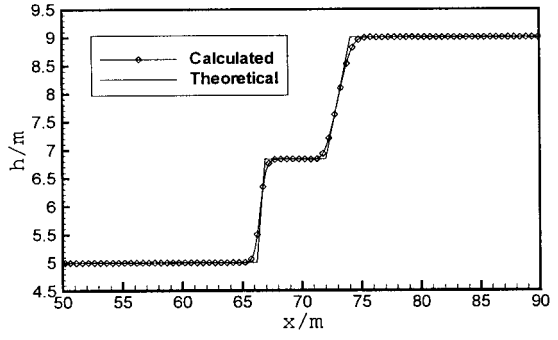

Figure 23. Comparison between analysis and computation of water level of water shock wave in a straight channel.

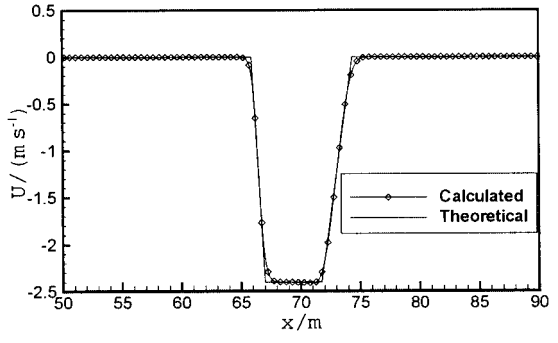

Figure 24. Comparison between analysis and computation of water velocity of water shock wave in a straight channel.

In Figure 25 there are three measurement stations, one of them is set on the entrance of the straight channel, the second and third stations are located at $\theta = 45°$ and 90° of the curved channel respectively. As water waves pass through the curved channel, the water levels on the outside and inside of the curved channel are different, so there are two measurement points at every measurement station. The grid number in this numerical example is near 7000. The grids are coarse in the water bank and fine in the channel. Figure 27 shows the comparison between the numerical results and measurement data. It is found that the agreement in the straight part of the channel is satisfied, but the difference in the curved channel is large. We find that there are also some differences in Dammuler *et al.*'s [23] and Molls and Chaudry's [24] numerical results. Maybe there are some unclear reasons in this problem, which can be the friction of the side walls of the channel is ignored, the flow in the channel cannot be described with shallow water wave equations because of its narrow width of channel and large water depth, conditions in the experiment are not simulated completely, and so on.

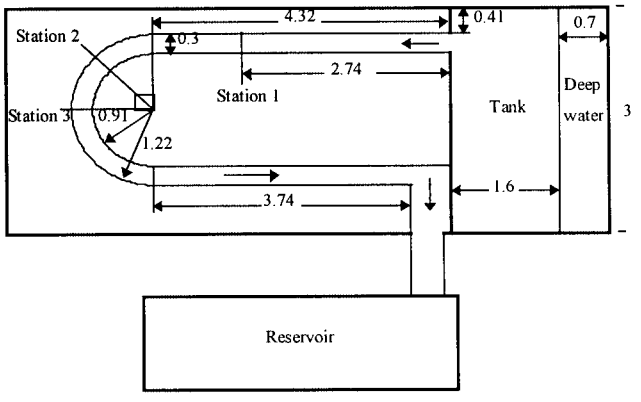

Figure 25. Sketch of measurement installation.

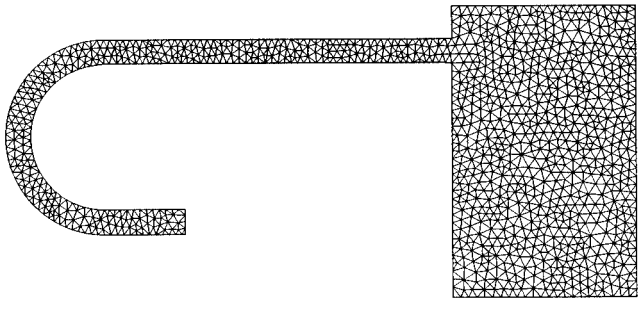

Figure 26. Domain and meshes of computation.

6.3. Climb of a soliton wave on slope

This numerical example is used to check the treatment method of the moving boundary condition. Figure 28 shows a channel with slope of $\alpha = 15°$, the left part of the channel has a horizontal bottom, the slope starts at point B. The equation of the soliton wave at $t = 0$ is

$$S(x, 0) = A \sec h^2\left(\sqrt{\frac{3A}{4h_\infty}}\,\frac{x - x_a}{h_\infty}\right) \tag{58}$$

The wave is moving along the x-direction with velocity $a_0 = \sqrt{g(h_\infty + A)}$, where A is an initial height of the wave, x_a is a given initial location that is zero. The initial wave level is as follows:

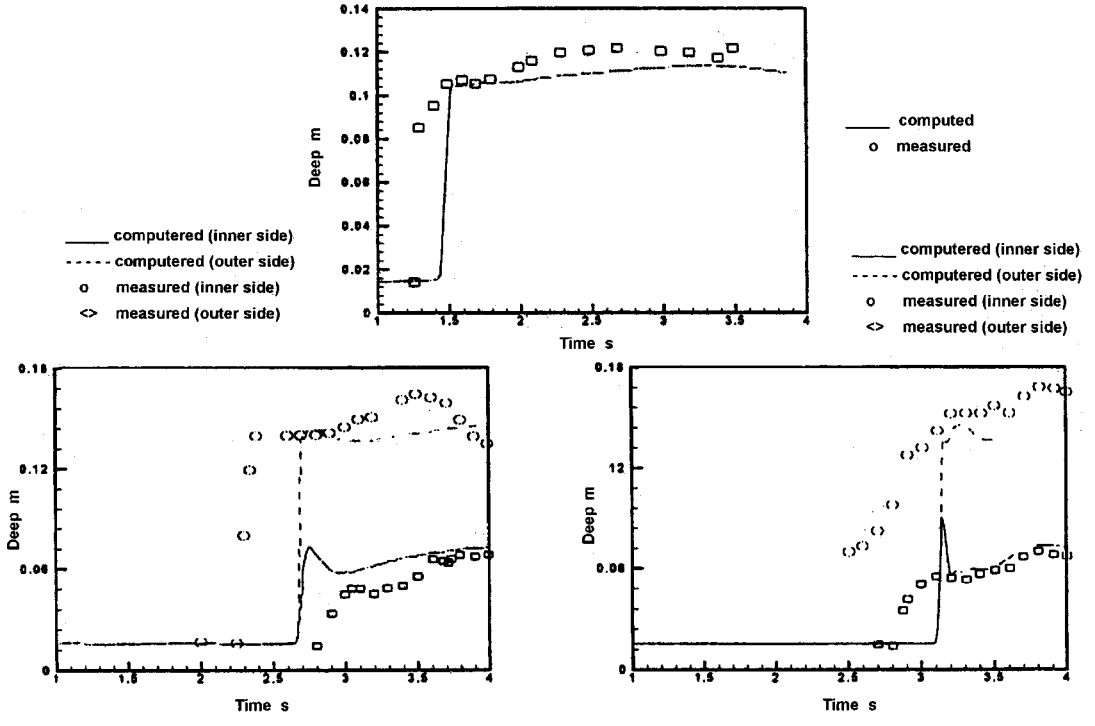

Figure 27. Comparison between experiment and computation of dam break in curve channel.

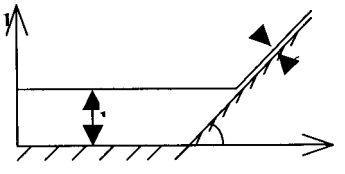

Figure 28. Sketch of moving bound

$$\begin{cases} h_i = S(x_i, 0) + \delta \\ h_i = \delta \end{cases}; \qquad \begin{cases} u_i = a_0 S(x_i, 0)/(S(x_i, 0) + h_\infty) \\ u_i = 0 \end{cases}; \qquad \begin{cases} v_i = 0, & x_i < x_B \\ v_i = 0, & x_i \geq x_B \end{cases} \tag{59}$$

where i is the order number of triangle elements and x_i is the x-coordination of the centre of the ith triangle element. In the present example, $A = 1$ m, the initial point of slope locates at $x = 60$ m, $h = 5$ m, $v_i = 10.5$, $\delta = 0.002$ m. The wave shapes at different times are displayed in Figure 29. They are similar to the result in Reference [9]. In Figure 30 the maximum heights of a wave on the slope at different times obtained by experiment and computation are

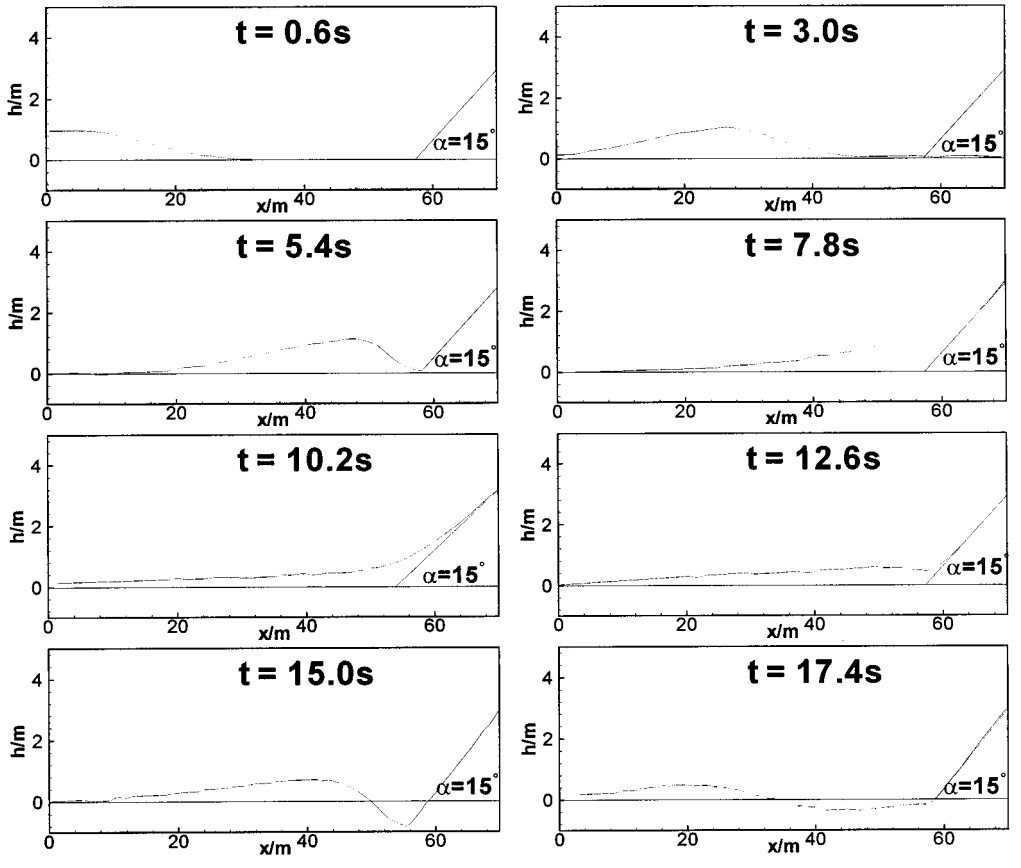

Figure 29. Evolution of water level of solitary wave climb.

compared. The agreement satisfactory. It shows that this treatment method of moving boundary condition is satisfactory and can be used in the numerical simulation of tidal bore in Hangzhou Gulf. (Note in Figure 30, the angle of slope is enlarged for visualization.)

6.4. Numerical simulation of tidal bore in Hangzhou Gulf

6.4.1. Approximate results with flat bottom. As we know, there are many factors that affect the generation of the tidal bore. The main factors are the shape of the gulf and the topography of the bottom surface. To distinguish their roles, the bottom of the gulf is assumed to be a horizontally flat, i.e. the influence of the land form of the bottom is ignored in the first step.

In the present paper, the depth of the bottom is 2 m (mean depth of gulf). Figure 31 shows the unstructured grid system, in which there are 7300 elements. The scale of elements is about 500 m. The tributary the Cao-er river is ignored because its influence is small. In our computation, the bound of region can be more complex with some tributaries.

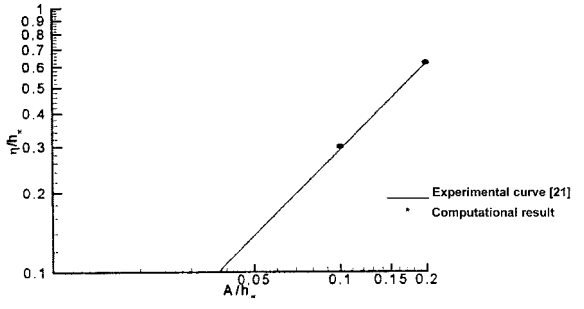

Figure 30. Comparison of maximum climb heights.

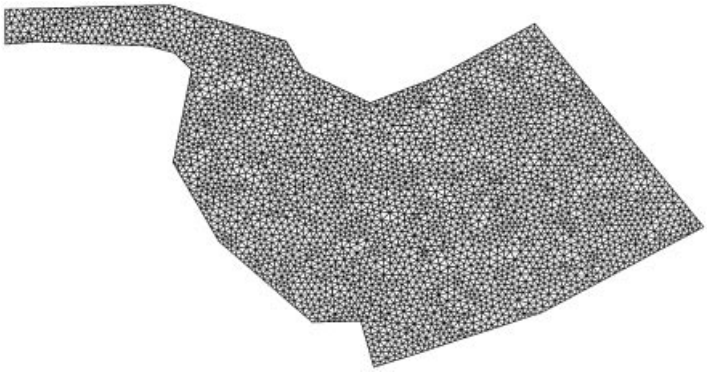

Figure 31. Meshes in computational domain of Qiantangjiang river (7300 triangles).

Here the Chezy coefficient is 500 $m^{1/2} s^{-1}$ and $dt = 0.01$ (equivalent to 10 s). On a PC486/66, the CPU time of every step is 16.7 s. The initial condition of velocity and water level are determined arbitrarily. The results in the initial stage are incorrect and are affected by the initial conditions, therefore they are ignored. The results shown in Figure 32 are the vectors of velocity and contours of water level that we can observe for the one straight-line tidal bore formation, development and disappearance. As water flows inward, the rudiment of tidal bore is formed after Ganpu and it becomes a clear tidal bore near Shuweishan. It agrees with the results of the observation. After that, the tidal bore develops continuously and it becomes more complex. After it reaches the corner on the north coast, the situation changes. The strength of tidal bore near the north is somewhat weakened and the south coast is strengthened. It is caused by the extruding of the south coast and the convergence of the upstream water surface width of the gulf. The weakened north tidal bore marches continuously and goes

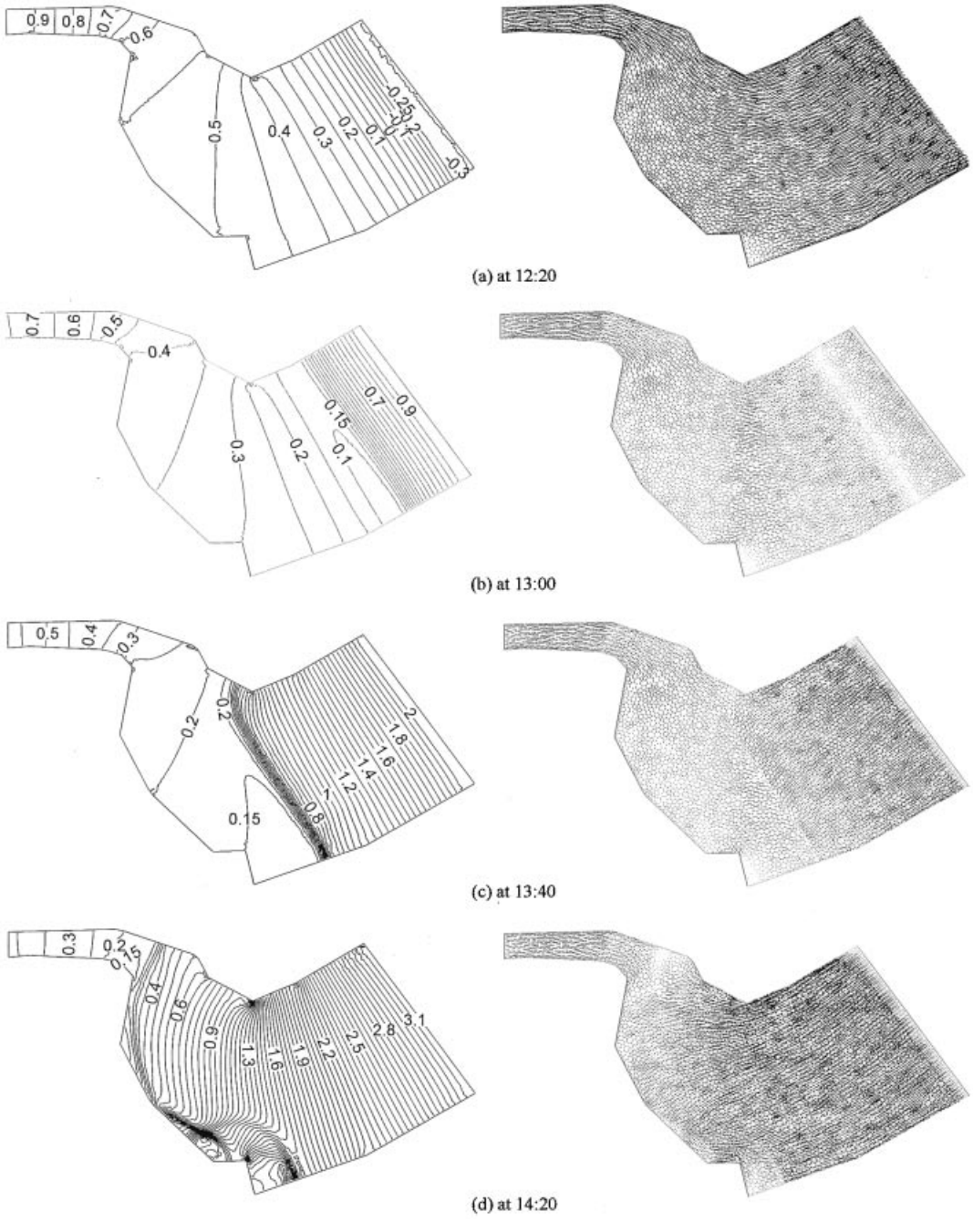

Figure 32. Contour of water level and velocity vector.

to the Qiantangjiang river, but the south tidal bore is reflected and moves to the other coast and forms a strong reflecting wave. The reflected wave goes upward and catches up with the weakened tidal bore to form a stronger tidal bore. This phenomenon is coincident with observation. Besides, by means of observation at different times, the speed of the tidal bore's propagation can be estimated, which is 5 $m\,s^{-1}$ approximately. This value agrees with the observation value.

From the flow vector figure we find that the speed near the tidal bore is about zero. This comes from the fact that the shallow water wave equation is depth averaged. Though the tidal bore has major upstream speed, this is only the movement of the surface layer of water and the lower layer water flows downstream. So the whole average flow speed approaches zero. After the tidal bore, the maximum value of fluid velocity is approximately 4.8 $m\,s^{-1}$. From the vector figure, one can find the wall boundary condition is ensured. In the computation, the conservation of fluid flow is checked. The maximum error is less than 5 per cent of momentum flux, which is a satisfactory result in engineering means.

In the present work, two unstructured grid systems are used, namely 7300 and 1500 grids respectively. It is found that the tidal bore appears clearly when the fine grid system is used. It is expected that the tidal bore will be more clear when the finer grid system is used. Besides, there is another suggested method, i.e., the adaptive unstructured grid system. Because this program runs on a PC486/66 and the CPU time of the computer is too long, the adaptive grid method is not used. This work will be carried out in the future.

Using a non-reflective boundary condition, the variance of water level at Yanguan (entrance) with time can be calculated. Figure 33 compares the calculated and observed variances. The agreement is satisfied.

Although the horizontal bottom is assumed, the computational results coincide with measurement results approximately. That means the construction of the gulf from exit to entrance is the main reason the tidal bore forms and the variance of topography of the bottom has a secondary role in forming the tidal bore.

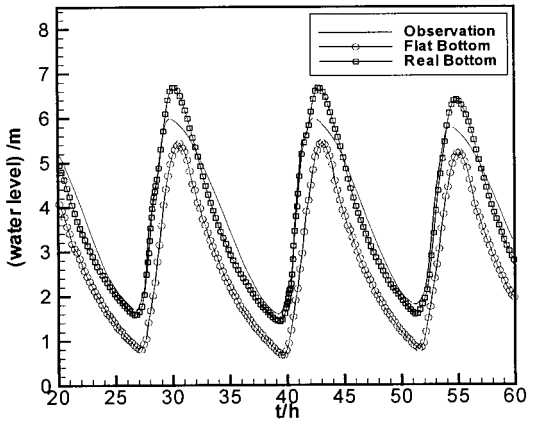

Figure 33. Comparison between computational and observational results.

6.4.2. Computational results with real bottom. In the real topography of the bottom of the Hangzhou Gulf, there are deep pools of 20–30 m, isolated islands and shoals that outcrop over the water surface. When the tidal bore occurs they are submerged in water. This complex topography of the bottom does not satisfy the basic assumption of the Saint-Venant equation. In the present computation, it is found that the calculation cannot be completed because of large and irregular variances of the gradient of the bottom. Therefore, the land form at the bottom should be smoothed, so the main character of the topography is reflected. After that there is no location with large gradients. Figure 34 shows the contours of depth of the smoothed bottom.

In the computation, the same unstructured grid system is used. Figure 35(a)–(d) show the velocity vectors and contours of the water level. In these figures we find that shoals outcrop over water surfaces or are submerged in water. The tidal bore is the same as the flat bottom situation in the initial stage. Then due to the existence of shoals, the river becomes narrow and the tidal bore develops faster and stronger; the high drop between water levels on both sides of the tidal bore is larger than that in the horizontal bottom.

Of course, the maximum height drop of the tidal bore in the numerical results is only more than 1 m. The reason is the grid scale is 500 m but the real height drop of the tidal bore is in 3–4 m. In the one-dimensional simulation, the height drop of the tidal bore is 3–4 m, where the adaptive grid is used and the minimum grid scale is only 5 m approximately. So we believe that an accurate result can be obtained when the adaptive unstructured grid system is used, the scale of the small elements located on both sides of the tidal bore is near 10 m and the program runs on a supercomputer with more memory and higher speed.

The computational variance of the water level at Yanguan according to the variety depth bottom is shown in Figure 33 also. We find there are no large differences between the two computational results except for the water level. It means that the tidal bore becomes stronger. It is clear that the bottom becomes shallower and shallower along the upward direction.

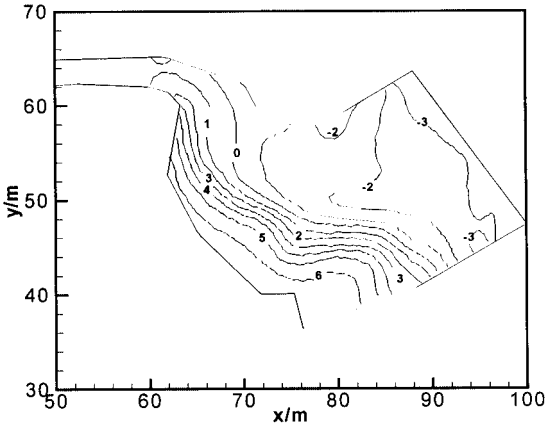

Figure 34. Topography of bottom result for Qiantangjiang at Yanguan river (approximation).

7. CONCLUSION

In the present paper, the unstructured grid system and the NND difference scheme are used in the numerical simulation using the shallow water wave equation. According to the examination of some one- and two-dimensional typical examples and the simulation of tidal bore in the Hangzhou Gulf and Qiantangjiang river, we reach the following conclusions:

1. The numerical results show that NND difference scheme can catch the stronger discontinuous in both one- and two-dimensional cases. In the one-dimensional numerical examples of water jump and dam-break, results show that this method can simulate the water wave motion with discontinuous jump, and it has good conservation. In the two-dimensional cases, the NND difference scheme can catch strong discontinuous in water waves too, e.g. dam-break, water jumps and tidal bores.
2. The finite volume method applied in the unstructured grid system can assure the conservation law.

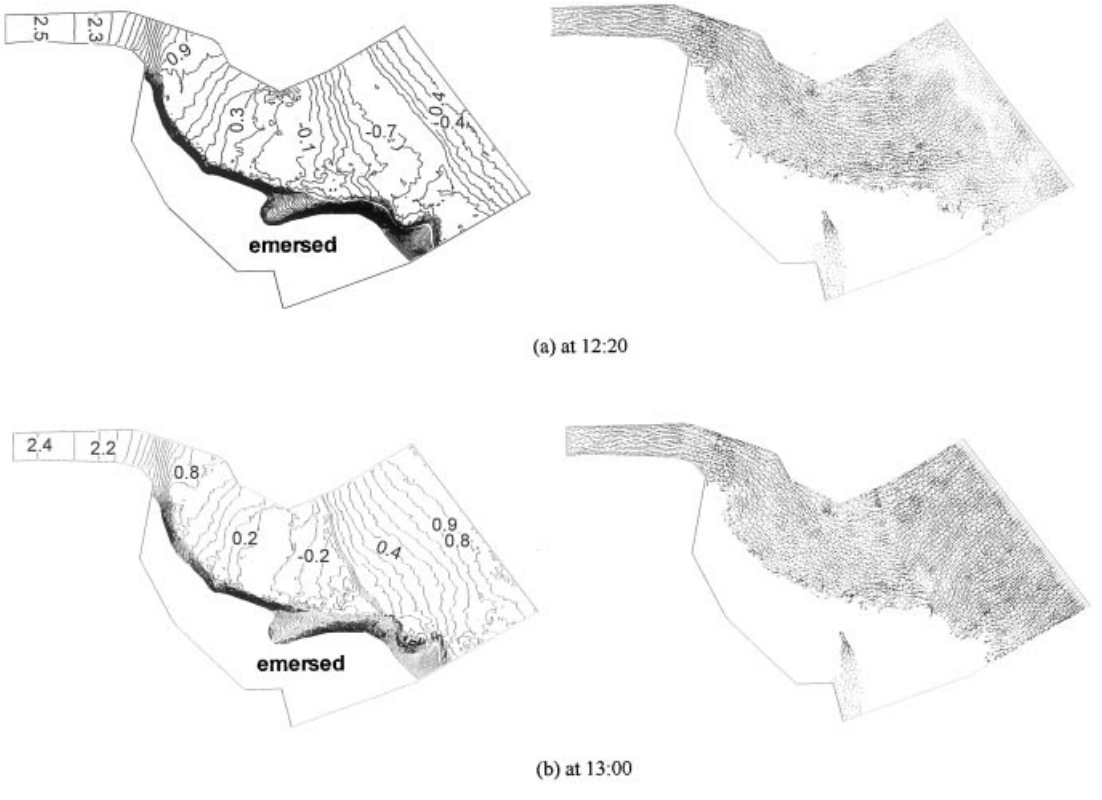

Figure 35. Contour of water level and velocity vector.

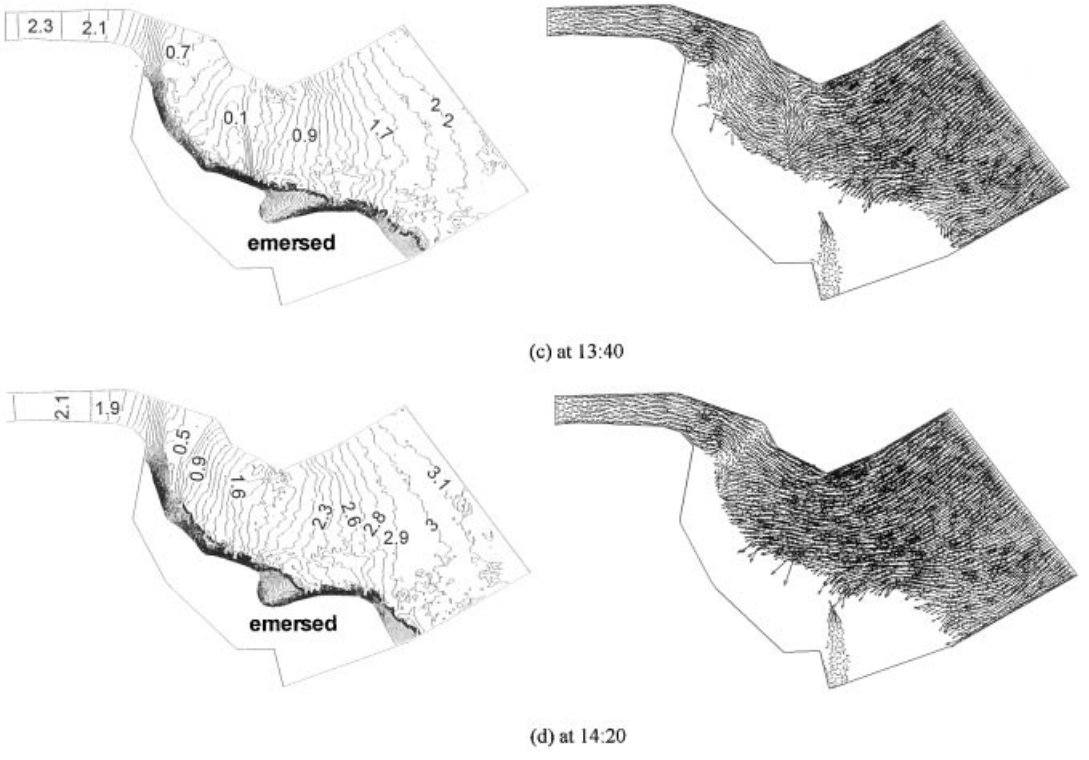

Figure 35 (*Continued*)

3. The non-reflective boundary condition at the entrance and the characteristic boundary condition are effective.
4. Adding an equation of kinematic energy to the shallow water equation is convenient for performing the flux-split of Saint-Venant equations. This kind of flux-split method is useful to ensure the computation stability and the application of NND scheme.
5. In the one-dimensional simulation of the tidal bore in the Qiantangjiang river, the water level difference between the computational result and the observed result is less than 0.2 m by adjusting the Chezy coefficient. There are few observed data and they are displayed in Figures 16–19 with lines or points. (In other positions, there are no observed data for comparison.) The numerical results of the simulation of Qiantangjiang tidal bore agree with the observed results after introducing the influences from the tributaries. The considerations of the in-discharge of tributaries and the method of adaptive mesh are available.
6. From the computational result, the tidal bore is caused mainly by the trumpet shape of the Hangzhou Gulf. Although the influence of the topography of the bottom is secondary, it still can not be ignored. It causes a stronger tidal bore as the bottom becomes shallower and shallower.

Though we have obtained some satisfactory results and reasonable conclusions, there are many areas to be improved. Due to the limit of memory and speed of the PC, the present results are preliminary. The adaptive grid should be used. The method to reflect the feature of the bottom correctly is another important problem in further investigation.

ACKNOWLEDGMENTS

This work is supported financially by Institute of River and Coast in Hangzhou. The authors thank Professor Han and Senior Engineer B.R. Lin of this institute for very useful discussion. The work of Dr Hon is supported by RGC Grant No. 9040286. Further, they would like to thank the reviewers for their valuable comments.

APPENDIX A

Now we prove that the NND scheme is also a TVD scheme.

Total variation of u^n is

$$TV(u^n) = \sum_j |u^n_{j+1} - u^n_j| = \sum_j |\Delta u^n_{j+1/2}| \tag{A1}$$

Set

$$S_{j+1/2} = \begin{cases} 1 & \text{if } \Delta u^n_{j+1/2} \geq 0 \\ -1 & \text{if } \Delta u^n_{j+1/2} < 0 \end{cases} \tag{A2}$$

then Equation (A1) can be rewritten

$$TV(u^n) = \sum_j S_{j+1/2} \Delta u^n_{i+1/2} \tag{A3}$$

Thus

$$\frac{\partial [TV(u^n)]}{\partial t} = \sum_j S_{j+1/2} \left[\frac{\partial u^n_{j+1}}{\partial t} - \frac{\partial u^n_j}{\partial t} \right] \tag{A4}$$

Equation (11) is

$$\begin{aligned} \left(\frac{\partial u}{\partial t}\right)^n_j = \left(\frac{\partial u_j}{\partial t}\right)^n = & -\frac{1}{\Delta x}(\Delta f^{+\,n}_{j-1/2} - \Delta f^{-\,n}_{j+1/2}) - \frac{1}{2\Delta x}\,\mathrm{minmod}(\Delta f^{+\,n}_{j-1/2}, \Delta f^{+\,n}_{j+1/2}) \\ & + \frac{1}{2\Delta x}\,\mathrm{minmod}(\Delta f^{+\,n}_{j-3/2}, \Delta f^{+\,n}_{j-1/2}) + \frac{1}{2\Delta x}\,\mathrm{minmod}(\Delta f^{-\,n}_{j+1/2}, \Delta f^{-\,n}_{j+3/2}) \\ & - \frac{1}{2\Delta x}\,\mathrm{minmod}(\Delta f^{-\,n}_{j-1/2}, \Delta f^{-\,n}_{j+1/2}) \end{aligned}$$

According to the definition of minmod(x, y), the above equation is

$$\left(\frac{\partial u}{\partial t}\right)_j^n = -\frac{1}{\Delta x}(\Delta f_{j-1/2}^{+n} - \Delta f_{j+1/2}^{-n}) - \frac{1}{2\Delta x} k_1 \Delta f_{j-1/2}^{+n} + \frac{1}{2\Delta x} k_2 \Delta f_{j-1/2}^{+n} + \frac{1}{2\Delta x} k_3 \Delta f_{j+1/2}^{-n} - \frac{1}{2\Delta x} k_4 \Delta f_{j+1/2}^{-n} \tag{A5}$$

where

$$0 \le k_i < 1, \quad i = 1, 2, 3, 4$$

Then, Equation (A5) becomes

$$\left(\frac{\partial u}{\partial t}\right)_j^n = -\frac{1}{\Delta x}\alpha \Delta f_{j-1/2}^{+n} - \frac{1}{\Delta x}\beta \Delta f_{j+1/2}^{-n} \tag{A6}$$

where

$$\begin{cases} \alpha = 1 - \dfrac{1}{2}(k_2 - k_1) \\ \beta = 1 - \dfrac{1}{2}(k_3 - k_4) \end{cases}$$

and

$$\alpha, \beta \ge \frac{1}{2}$$

On the other hand, Equation (A6) can also be rewritten as follows:

$$\left(\frac{\partial u}{\partial t}\right)_j^n = -\hat{\alpha}_{j-1/2} \Delta u_{j-1/2}^n + \hat{\beta}_{j+1/2} \Delta u_{j+1/2}^n \tag{A7}$$

where

$$\hat{\alpha}_{j-1/2} = \frac{\alpha}{\Delta x} \frac{f_j^{+n} - f_{j-1}^{+n}}{u_j^n - u_{j-1}^n}, \qquad \hat{\beta}_{j+1/2} = \frac{\beta}{\Delta x} \frac{f_{j+1}^{-n} - f_j^{-n}}{u_{j+1}^n - u_j^n}$$

Due to

$$\frac{\partial f^+}{\partial u} = a^+ \ge 0, \qquad \frac{\partial f^-}{\partial u} = a^- \le 0$$

and

$$\frac{f_j^{+n} - f_{j-1}^{+n}}{u_j^n - u_{j-1}^n} \geq 0, \qquad \frac{f_{j+1}^{-n} - f_j^{-n}}{u_{j+1}^n - u_j^n} \leq 0$$

then

$$\hat{\alpha}_{j+1/2}, \hat{\beta}_{j+1/2} \geq 0 \tag{A8}$$

By substituting Equation (A7) into Equation (A4), we obtain

$$\frac{\partial TV(u^n)}{\partial t} = \sum_j S_{j+1/2}\{-\hat{\alpha}_{j+1/2}\Delta u_{j+1/2}^n + \hat{\beta}_{j+3/2}\Delta u_{j+3/2}^n + \hat{\alpha}_{j-1/2}\Delta u_{j-1/2}^n - \hat{\beta}_{j+1/2}\Delta u_{j+1/2}^n\}$$

$$\frac{\partial TV(u^n)}{\partial t} = -\sum_j v_{j+1/2} S_{j+1/2}\Delta u_{j+1/2}^n = -\sum_j v_{j+1/2}|\Delta u_{j+1/2}^n| \tag{A9}$$

where

$$v_{j+1/2} = \hat{\alpha}_{j+1/2}\left(1 - \frac{S_{j+3/2}}{S_{j+1/2}}\right) + \hat{\beta}_{j+1/2}\left(1 - \frac{S_{j-1/2}}{S_{j+1/2}}\right)$$

By Equations (A2) and (A9) we have $v_{j+1/2} \geq 0$.

So

$$\frac{\partial TV(u^n)}{\partial t} \leq 0$$

The NND scheme is TVD scheme.

REFERENCES

1. Matsoukis PFC. The application of the method of characteristics for the simulation of nearly horizontal flow in two and three spatial dimensions condition. *International Journal for Numerical Methods in Fluids* 1992; **14**: 379–401.
2. Tan WY, Han ZC. Two-dimensional numerical simulation of the tidal bore in Hangzhou Gulf. Nanjing Institute of Hydrology and Water Source, The Institute of Coast and Estuarine, Report 93-05, 1993.
3. Casulli V. Semi-implicit finite difference methods for the two-dimensional shallow water equations. *Journal of Computational Physics* 1990; **86**: 54–74.
4. Fennema RJ, Chaudhry MH. Implicit methods for two dimensional unsteady free-surface flows. *Journal of Hydraulic Engineering* 1989; **27**(8): 321–332.
5. Fennema RJ, Chaudhry MH. Explicit methods for two dimensional transient free-surface flows. *Journal of Hydraulic Engineering* 1990; **116**(8): 1013–1034.
6. Spitaleri RM, Corinaldesi L. A multigrid semi-implicit finite difference method for the two-dimensional shallow water equations. *International Journal for Numerical Methods in Fluids* 1997; **25**: 1229–1240.
7. Walters RA. A finite element model for tides and currents with field applications. *Communications in Applied Numerical Methods* 1988; **4**: 401–411.

8. Westerink JJ, Connor JJ, Stolzenbach KD. A frequency–time domain finite element model for tidal circulation based on the least squares harmonic analysis method. *International Journal for Numerical Methods in Fluids* 1988; **8**: 813–843.
9. Westerink JJ, Luettich RA, Baptista A, Scheffner NW, Farrar P. Tide and storm-surge predictions using finite element model. *Journal of Hydraulics Engineering—ASCE* 1992; **118**(10): 1373–1390.
10. Westerink JJ, Luettich RA Jr, Baptista AM, Scheffner NW, Farrar P. Tide and storm surge predictions using finite element model. *Journal of Hydraulic Engineering* 1994; **118**(10): 1373–1390.
11. Westerink JJ, Luettich RA Jr, Muccino JC. Modeling tides in the western North Atlantic using unstructured graded grids. *Tellus* 1994; **46A**: 178–199.
12. Westerink JJ, Luettich RA Jr, Wu JK, Kolar RL. The influence of normal flow boundary conditions on spurious modes in finite element solutions to the shallow water equation. *International Journal for Numerical Methods in Fluids* 1994; **18**: 1021–1060.
13. Toshio K, Kawasaki T, Kawahara M. Finite element method for shallow water equation including open boundary condition. *International Journal for Numerical Methods in Fluids* 1991; **13**: 939–953.
14. Kolar RL, Westerink JJ, Cantekin ME, Blain CA. Aspects of nonlinear simulations using shallow-water models based on the wave continuity equation. *Computers in Fluids* 1994; **23**(3): 523–538.
15. Kolar RL, Gray WG, Westerink JJ. Boundary conditions in shallow water models an alternative implementation for finite element codes. *International Journal for Numerical Methods in Fluids* 1996; **22**: 603–618.
16. Lardner RW. Optimal control of open boundary conditions for a numerical tidal model. *Computer Methods in Applied Mechanics and Engineering* 1993; **102**: 367–387.
17. Peterson RC, Jimack PK, Kelmanson MA. The solution of two-dimensional free surface problems using automatic mesh generation. *International Journal for Numerical Methods in Fluids* 1999; **31**: 937–960.
18. Zhang HX. NND difference scheme. *Journal of Aerodynamics* 1998; **1**(1): 1–12.
19. Tan WY, Hu SY. One-dimensional computation of unsteady flow in natural river with conservation scheme. *Advances in Water Science* 1990; **1**(1): 23–31.
20. Thompson KW. Time dependent boundary conditions for hyperbolic systems. *Journal of Computational Physics* 1987; **68**: 1–24.
21. Hall JV, Watts GM, Army US. Corps of Engineering, Beach Emotion Board. Technical Memo. Vol. 33, 1953.
22. Miller S, Chaudry MH. Dam-break flows in curved channel. *Journal of Hydraulic Engineering* 1989; **115**(11): 1465–1478.
23. Dammuler KW, Bhallamudi SM, Chaudhry MH. Modeling of unsteady flow in curved channel. *Journal of Hydraulic Engineering* 1989; **115**(11): 1479–1495.
24. Molls T, Chaudry MH. Depth-averaged open-channel flow model. *Journal of Hydraulic Engineering* 1995; **121**(6): 453–465.

